SCHOOL OF ENGINEERING

Analysis and Behaviour of Structural Concrete Reinforced with Sustainable Materials

Thesis submitted in accordance with the requirements of the University of Liverpool for the degree of Master in Philosophy in Civil and Structural Engineering

Luna Salh

February 2014

Abstract

Fibre reinforced polymer (FRP) composites have extensive applications in various fields such as the aerospace and automotive engineering industries. In recent years, there have been more novel applications for FRP in the construction industry. FRP is known for its beneficial properties such as high strength to weight ratio, lower specific weight and excellent corrosion and fatigue resistance. These advantages have made FRP more desirable to be used as an alternative to steel reinforcement for internal as well as external reinforcement in structural concrete, especially those which are exposed to extreme environments.

One of the objectives of this research is to identify all the different types of fibre reinforced polymer such as CFRP, GFRP and BFRP. These all can be used as an alternative to conventional steel reinforcement in structural concrete. For each type their physical and mechanical properties such as tensile strength, modulus of elasticity, ultimate strain, durability in alkaline environments, fatigue strength and bond strength has been identified.

This thesis also presents the results of experimental, analytical and numerical modelling investigations of the performance and behaviour of concrete members reinforced with basalt fibre reinforced polymer (BFRP). The primary objective of this research is to address the applicability of this material as internal reinforcement and to investigate the applicability of current FRP design guides on BFRP as an internal reinforcement to structural concrete members.

For the flexure investigation of BFRP reinforced concrete sections, four beams were studied, two of them being BFRP reinforced beams and two of them being conventional steel reinforced beams that have been used as control beams. The outcome of this has shown us different types of FRP bars that can replace the traditional steel reinforcement in concrete structures. Also it provides us with detailed knowledge of the behaviour of materials such as BFRP bars. Moreover, it determines the applicability of current FRP design guidelines on BFRP reinforcements.

Acknowledgments

First and foremost, I would like to thank my academic advisors, Dr. Stephen Jones for his guidance and support throughout this project. His motivation, encouragement, dedication, positive mind, and valuable advice made it a very exciting and invigorating experience. I also would like to thank Dr. Zhongwei Guan.

I would like to thank Mr. Dave Hunter for his effort in constructing the beams. Finally, my deepest thanks to my dearest husband Swara, for his financial and emotional support and understanding during all this time and my lovely kids Alan and Miran.

Contents

1. Introduction

Structural concrete is usually reinforced with conventional steel bars, which can last for decades without exhibiting any deterioration if it is properly protected from corrosion attack. However this is not possible in so many cases, such as structures that are exposed to extreme environments such as de-icing salts in bridge, marine structures, parking structures, bridge decks, highway under extreme environments, etc. The combination of moisture contaminated with chlorides and temperature will accelerate the corrosion of steel reinforcement and lead to the deterioration of the structure and eventual loss of serviceability.

The corrosion of steel reinforcement in concrete structures is the main factor in reducing the lifespan of these structures. The repair and retrofitting of these structures may cost as much as twice its original cost. In general, it has been estimated that approximately 15% of all bridges are deficient structurally, mainly due to the corrosion of the steel reinforcement. The annual direct cost for repairing these structures are estimated to reach $8.3 billion in the United States alone [1]. In Canada, the cost of repairing steel reinforced concrete structures is estimated to be around $74 billion [2]. In Europe it has been estimated that the cost of steel corrosion is around $3 billion a year [3]. In India the annual cost of corrosion is around $30 billion. While in the UK it is estimated that over £300 million is spent annually to repair and rehabilitate the existing infrastructure [4].

To overcome the corrosion problems and increase the lifespan of reinforced concrete structures a variety of techniques are used worldwide, such as protective coatings and linings, metallic coating and claddings, corrosion resistance alloys, corrosion inhibitors, cathodic and anodic protection, using stainless steel bars and corrosion resistance composites [5]. However, most of these solutions have either had failures or are expensive. One of the preferred solutions in many countries is the use of fibre reinforced polymer (FRP) rebar as an internal reinforcement for concrete structures.

Fibre reinforced polymer (FRP) rebar is not metallic and so is not susceptible to corrosion and it is impervious to attack by chlorides. FRP rebar will eliminate the durability problems seen with steel reinforcement and increase the service life of the structure. Moreover, FRP rebar has a high tensile strength to weight ratio which makes it more cost effective that using conventional steel rebar.

FRP composite materials are typically made of fibres and resins. The most common fibres are carbon, glass, aramid and the most recently developed fibres are basalt fibres. The most common type of resins are epoxy, vinylesters, polyesters or phenolic thermosetting resins that have fibres fractions greater than 30% [6].

The main advantage of FRP reinforcement over conventional steel reinforcement is the high tensile strength of these bars which is three times higher than that of steel reinforcement. They also have improved chemical attack resistance, fatigue resistance, lower density (about a quarter that of steel), long term durability and corrosion resistance [6].

1.1 Significance

In this research all the different types of fibre reinforced polymer such as CFRP, GFRP and BFRP will be presented to identify the available products, their physical and mechanical properties such as tensile strength, modulus of elasticity, ultimate strain, durability, fatigue strength and bond strength.

The analysis and behaviour of structural concrete sections reinforced with sustainable materials as flexure reinforcement will be studied. Special attention will be paid to the reinforcing of concrete beams with basalt fibre reinforced polymer (BFRP). An ABAQUS model will be developed to study the detailed behaviour and analysis of basalt fibre reinforced polymer reinforcement for concrete beams.

1.2 Objectives

The main objectives of this research study can be summarised as follows:

1. To identify and classify all available alternative reinforcing materials that could be used as reinforcement in structural concrete.
2. To compare their physical and mechanical properties.
3. To investigate the design methods for using these products as an alternative to steel reinforcement.

4. To investigate the applicability of current design guides on BFRP bars or Rock Bars.
5. To develop a finite element model of a BFRP RC beam by using ABAQUS and use it to study further parameters.

1.3 Research Methodology

- Experimental: the aim of the experimental work is to test concrete beams reinforced with BFRP bar to simulate the probability of using BFRP as an alternative to steel reinforcement in concrete members. The experiments consist of casting two beams (of dimensions 150x200x2000 mm) reinforced with BFRP in the tension zone. The resulting beams will be subjected to four point flexure tests.
- Analytical: Sectional analysis using the strain compatibility method is used in this study. Since basalt is a relatively new material in structural engineering, there is a lack of design guidance. Therefore, the ACI design guide for FRP reinforcements is applied to analyse the concrete section reinforced with BFRP bars. Also a finite element nonlinear analysis is carried out by computer simulations using the Abaqus program to verify the experiments.

1.4 Thesis Outline

- Chapter 2 presents more details on the literature review of mechanical and material properties of FRP bars, as well as on the main approaches used by the existing guidelines for the design of FRP RC structures. It also presents the ultimate limit state design principles for flexure and the serviceability limit states as the basis of document ACI 440.1R-06.
- Chapter 3 presents the experimental programme on the basalt fibre reinforced polymer (BFRP) reinforced concrete beams.
- Chapter 4 presents the background of crack modelling of reinforced concrete beams and sectional analysis using ABAQUS.
- Chapter 5 compares the experimental and analytical results.

- Chapter 6 summarizes the main conclusions, and the overall findings of this project with recommendations for further actions to be taken.

2. Literature Review

This chapter provides a comprehensive review of the literature on the alternative materials such as FRP bars that can be used as reinforcement in structural concrete sections to replace the conventional steel reinforcement. Consideration will be given to their mechanical and physical properties, advantages and disadvantages and an investigation into the design philosophy and design guides. Since BFRP is a new material; further study is required to understand the mechanical and physical properties, its formation, application, advantages and disadvantages. The applicability of the current ACI design guides to predict the flexure behaviour of structural sections reinforced with BFRP will be investigated.

2.1 History of FRP Reinforcement

The idea of making composite materials by combining two different materials is not new and can be dated back to the ancient Egyptians when they used straw to reinforce their mud and make a stronger composite material. Fibre reinforced polymer is just a later version of this idea [7].

The use of Fibre Reinforced Polymer (FRP) goes back to the 1950's after World War II in various fields such as aerospace and automotive industries. Nowadays different parts of today's vehicles are made of composites, and many large parts of modern aircraft are made out of composites as they are lighter and more fatigue resistance compared to traditional materials.

Since the 1960s many highway bridges and structures have started to deteriorate due to the corrosion problems of the reinforcing steel as a result of road de-icing salts in colder climates or marine salts in coastal areas, which accelerated the corrosion of the reinforcing steel. Many efforts has been taken in the past to overcome the corrosion of steel reinforcement such as applying a galvanized coating to the surface of the reinforcing bars, the use of epoxy coated steel reinforcing bars in 1970s [8] and the use of stainless steel.

In the late 1960s, the Bureau of Reclamation in the US developed a programme for using polymer impregnated concrete but it was not possible to use steel reinforcement with polymer concrete due to the incompatibility in thermal properties. This led Marshall Vega to manufacture glass fibre reinforced polymer as reinforcement bars [8].

In 1980s in the USA a pultrusion company entered the FRP reinforcing bar industry under the name of International Grating, Inc [8]. They developed sand coated glass FRP bars followed by the development of deformed FRP bars by Marshall Composites Inc in the 1990s. These experiments started to be undertaken with carbon FRP with deformed and sand coated surfaces [5].

In the late 1980's the use of this composite material expanded widely into civil and structural engineering in Japan, United Kingdom and the US. Since then they have developed into economically and structurally viable construction materials for buildings, bridges and other applications which are in extreme chemical environments.

In Europe, particularly in Germany, FRP was first used as concrete reinforcement in the construction of a prestressed FRP bridge in 1986 [9]. From 1991 to 1996 the European BRITE/EURAM project has undertaken extensive research on testing and analysis of FRP [9].

In parallel to the USA's efforts in developing glass FRP, the Japanese also concentrated on the development of carbon FRP bars as reinforcement for structural concrete members in corrosive environments, due to the higher resistance of carbon FRP in alkaline environments.

There have now been many bridges constructed throughout Europe, Japan and USA that use FRP bar reinforcement. The transportation industries demand such as highways and bridges and the large demand for electrically nonconductive reinforcement in hospitals in magnetic resonance imaging (MRI) facilities for FRP reinforcement led the marketing for FRP even to expand more widely. In 1993 there were nine companies actively marketing commercial FRP reinforcing bars in the USA alone [8].

Due to the degradation performance of glass and aramid FRP within concrete in highly alkaline environments and the high cost of carbon FRP, there was a demand for producing another type of FRP bars for applications where corrosion is a problem. This new product was known as basalt FRP. In the United States, the first attempt to produce basalt fibres was in 1923 [10]. However, the first production of basalt fibres was in Kiev, Ukraine during

1980s. In 2000, Japan and Ukraine established a new enterprise for the production of basalt fibres. In addition to Japan, South Korea, China, Australia and the USA are working on developing basalt FRP [10].

2.2 FRP Bars

Fibre reinforced polymer (FRP) bars are structural bars made of continuous fibres held in a polymeric resin matrix. Together they contribute in the resulting mechanical and physical property which is required for specific structural applications.

The fibres used are continuous fibres with high strength and high stiffness, however they are comparatively lightweight. They provide the composite with the required strength. The most common type of fibres in structural purposes is carbon, glass, aramid, and more recently the use of basalt fibres. Due to the incompatibility in thermal properties of steel fibres with the matrix, steel fibres are not used for reinforcing the polymer.

The polymeric matrix binds the fibres and protects their surface from damage during handling, transporting, manufacturing, and the service life of the composite bars. In addition, the matrix plays an important role in the strength of the bars because it transfers the stress to the fibres through the matrix. Therefore it should be compatible with the fibres in terms of its thermal and chemical properties. The most common types of resin are epoxy, vinylesters and polyesters.

2.3 Currently Used FRP Bars

Currently different types of Fibre Reinforced Polymer (FRP) rebar for reinforcing concrete structures are available, which are classified by fibre type as shown in Figure 2.1.

1 Aramid Fibre Reinforced Polymer (AFRP) rebar.

   Aramid fibres were first produced under the name of Kevlar, and it was the first type of FRP tendon in the 1980s. Aramid fibres exhibit high moisture absorption, low melting temperatures, high initial cost and relatively poor compressive strength which made them less attractive for the use in the construction field. However AFRP's are lighter in weight compared to other types of FRP's and have higher energy absorption because of their high rupture strain and damping coefficient.

2 Carbon Fibre Reinforced Polymer (CFRP) rebar.

Carbon fibres compared to AFRP's can stand more heat and they do not absorb moisture. They have a very low thermal coefficient, which makes them desirable to be used in structures that are exposed to extreme temperatures. Carbon fibres are more attractive to be used in structural concrete reinforcement due to their high tensile strength and durability.

3 Glass Fibre Reinforced Polymer (GFRP) rebar.

Glass fibres can absorb moisture especially in salty and alkali environments. They are also sensitive to creep rupture under sustained stress. Therefore, its strength can be reduced by 60% of its ultimate strength in some cases. GFRP's do however have lower costs, higher chemical resistance and excellent in insulating properties which make them very attractive for use in building construction engineering.

4 Basalt Fibre Reinforced Polymer (BFRP) rebar.

Basalt fibres are a relatively new material to the field of structural engineering. Using basalt fibres as reinforcement within a polymer matrix (FRP) has become more popular in the past decade. They have been used as reinforcement in concrete directly and as FRP for internal reinforcement as bars and external strengthening as sheets. They have excellent chemical resistance which are environmentally and ecologically harmless. Also they have no adverse reactions with water and are not flammable. Basalt fibre rebar will be discussed in detail in this thesis.

[12].

Table 2.1 Advantages and Disadvantages of FRP Reinforcement [12]

Advantages of FRP reinforcement	Disadvantages of FRP reinforcement
High longitudinal tensile strength (varies with sign and direction of loading relative to fibre)	No yielding before brittle rupture
Corrosion resistance (not dependent on coating)	Low transverse strength (varies with sign and direction of loading relative to fibre)
Not magnetic	Low modulus of elasticity (varies with type of reinforcing fibre)
High fatigue endurance (varies with type of reinforcing fibre)	Susceptibility of damage to polymeric resins and fibres under ultraviolet radiation exposure.
Lightweight (about 1/5 to ¼ the density of steel)	Low durability of glass fibres in moist environments.
Low thermal and electrical conductivity (for glass and aramid fibres)	Low durability of some glass and aramid fibres in an alkaline environment.
	High coefficient of thermal expansion perpendicular to the fibres, relative to concrete.
	May be susceptible to fire depending on matrix type and concrete cover thickness.

2.5 Typical Applications

FRP reinforcing bars are anti-corrosion materials. Therefore; it is expected to find the applications in structures in or near marine environments, in or near the ground, in chemical or other industrial plants and in thin structural elements. The first application of using FRP reinforcements in concrete structures was in Japan, then many projects were developed in the early 90's, like floating marine structures Figure2.2, pontoon bridges Figure 2.3, non-magnetic structures such as tracks for linear motors Figure 2.4, bridge decks Figure 2.5, and ground anchors Figure 2.6.

Figure 2.2 Uses of Leadline Elements for the Tensioning of Diagonals of a Floating Marine, Japan

Figure 2.3 Use of FRP Tendons in the Pontoon Bridge at Takahiko Three Country Club, Japan

Figure 2.4 Magnetic Levitation Railway System in Japan

Figure 2.5 Uses of CFRP Bars in a Stress Ribbon Bridge at the Southern Yard Country, Japan

Figure 2.6 Uses of Technora Elements as Ground Anchors along the Meishin Expressway, Japan

Researches and development of FRP are undergoing in many other countries, most noticeably in USA, Canada and Europe. In Europe the first completely FRP reinforced footbridge was installed by the Eurocrete project in 1996, see Figure 2.7.

Figure 2.7 The First Concrete Footbridge in Europe with Only FRP Reinforcement (Euroctete Project)

In USA and Canada which are currently the country leaders in using FRP bars, mainly as reinforced concrete bridge decks reinforcements[13]. Figures 2.8 and 2.9 show some recent bridge applications in USA and Canada.

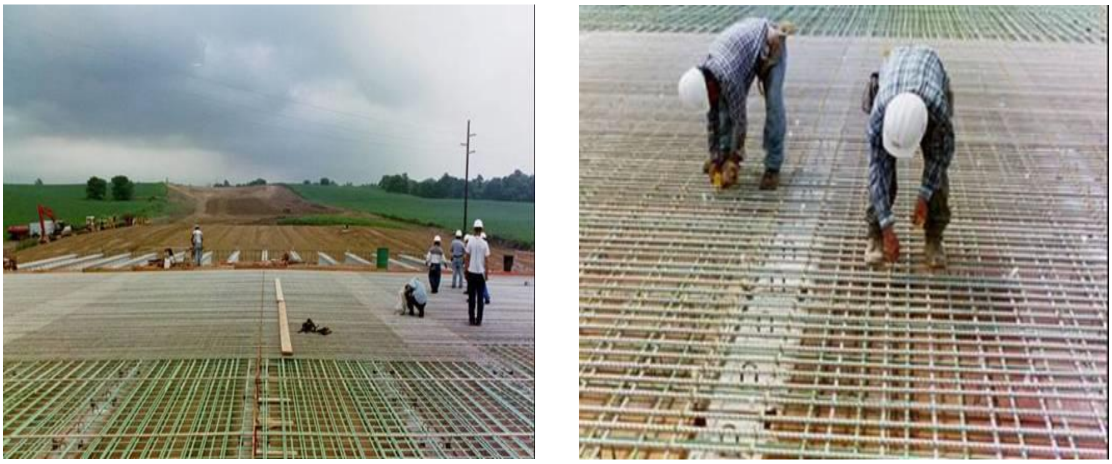

53rd Ave Bridge, City of Bettendorf – Iowa (USA) [14]

Sierrita de la Cruz Creek Bridge, Potter County – Texas (USA)[15]

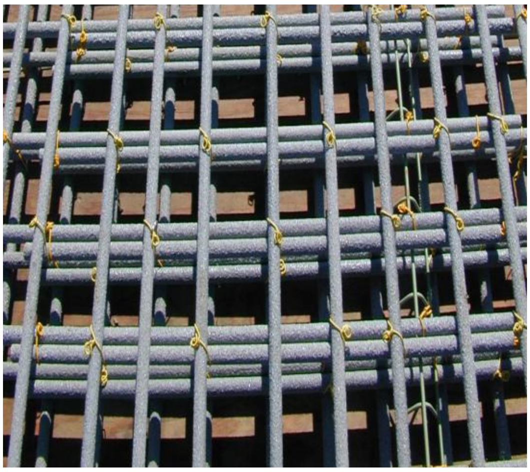

GFRP Bridge Deck, Morristown – Vermont (USA) [2002]

Figure 2.8 Recent Applications of FRP RC Bridge Decks in USA

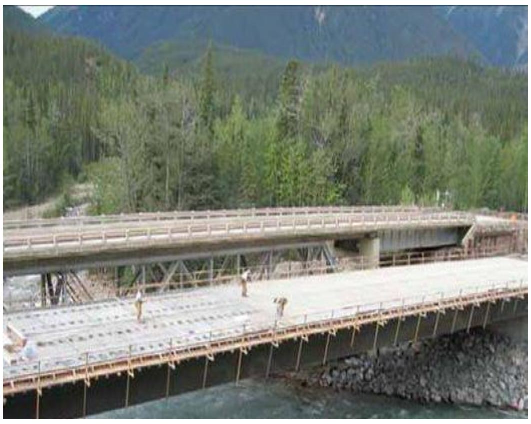

Trout River Bridge, AICAN Highway – British Columbia [2004]

GFRP Bridge Deck, Cookshire-Eaton – Quebec [2003]

Crowchild Bridge Deck, Calgary, Alberta[16]

GFRP Bridge Deck, Wotton, Quebec[16]

Figure 2.9 Recent Applications of FRP RC Bridge Decks in Canada

The use of FRP rebar for MRI hospital facilities has been very common. Due to the magnetic transparency of the rebar, any transient magnetic field will not be reflected by the reinforcement used in the concrete and negatively affect the quality of the MRI image, see Figure 2.10.

Lincoln General Hospital, Lincoln – NE (USA)

York Hospital, Trauma Centre (USA)

Figure 2.10 Recent Constructions of FRP RC Hospital Rooms for MRI

2.6 Properties

2.6.1 Mechanical Properties

The mechanical properties of a material are those properties that describe a reaction to an applied load. The mechanical properties of materials determine its range of usefulness and establish the service life that can be expected. They are also used to help classify and identify materials.

2.6.1.1 Tensile Strength, Tensile Modulus of Elasticity and Ultimate Strain

In general all the different types of Fibre Reinforced Polymer rebar behave linearly up to failure without exhibiting any yielding points or subsequent plastic behaviour. Figure 2.11 illustrates the typical stress-strain behaviour of FRP bars compared of that of steel.

In FRP bars the fibres are the main load carrying element, therefore the type, ratio and the orientation of these fibres play a big role in the strength of these bars. They also determine the rate of curing, the manufacturing process and quality control that is required.

The tensile properties of FRP rebar should be obtained from the manufacturer. The guaranteed tensile strength (f_u) is normally reported by the manufacturer and is defined as the mean strength- three standard deviations ($f_u = f_{u,ave} - 3\sigma$), and similarly for the rupture strain ε_{*fu} ($\varepsilon_{*fu} = \varepsilon_{u,ave} - 3\sigma$) The guaranteed modulus is defined as the mean modulus E_f ($E_f = E_{f,ave}$) as provided by the ACI code. Where, σ is standard deviation.

Below table gives the usual tensile properties of the most commonly used FRP bars are reported in ACI 440.1R-06.

Table 2.1: Comparison of Tensile Properties of Reinforcing Bars

	Steel*	GFRP*	CFRP*	AFRP*	BFRP**
Nominal yield stress (MPa)	276 – 517	N/A	N/A	N/A	N/A
Tensile strength (MPa)	483 – 690	483 – 1600	600 – 3690	250 -2540	1200
Elastic modulus (GPa)	200	35 – 51	120 – 580	41 – 125	50
Yield strain %	0.14 – 0.25	N/A	N/A	N/A	N/A
Rupture strain %	6.0 – 12.0	1.2 – 3.1	0.5 – 1.7	1.9 – 4.4	2.5

*Typical values for fibre volume fractions ranging from 0.5 to 0.7 (ACI 440.1R-03)

** Values for fibre volume fraction of 0.8 (www.magmatech.co.uk)

As the FRP bars are brittle materials and brake sharply without undergoing a deformation which known as necking in steel bars. Therefore, the cross section does not shrink along the bar, as a result FRP bars have a higher tensile strength property compared to steel.

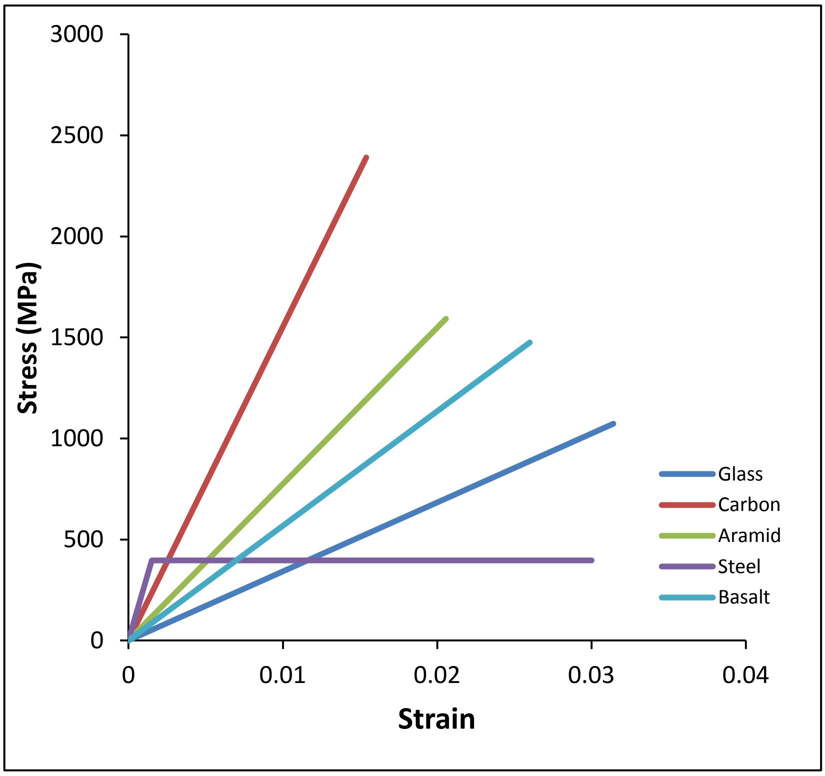

Figure 2.11 Stress-Strain curves for typical reinforcing bars [9]

2.6.1.2 Compressive Behaviour

FRP bars in the compression areas have very little contribution to the compressive strength of the section. Tests have shown that the compressive strength is lower that the tensile strength [17].

According to ACI 440.1R-03 [18] the compressive modulus of elasticity is approximately 80% for GFRP, 85% for CFRP, and 100% for AFRP of the tensile modulus of elasticity of the same product. For BFRP there isn't any recorded data up to date.

Unlike the tensile modulus of FRP rebar, the bar size, type, quality control and length to diameter ratio of the bars have an influence on the compressive modulus.

2.6.1.3 Bond Behaviour

The bond performance of FRP rebar will be affected by the manufacturing process of the bars, the environmental factors and the property of the bars [19]. Also the bond strength decreases as the diameter of the bars increases, similar to steel [20].

The bond can be transferred by:

- The chemical bond of the interface between the concrete and the bar (adhesion resistance).
- The friction resistance force due to the roughness of the FRP rebar surface.
- Mechanical interlock of the FRP rebar against the concrete.
- The pressure against the FRP bars which occurs due to the shrinkage of the concrete when it hardened and the swelling of the FRP bars due to moisture absorption and changes in temperature. In order to improve the bond strength between FRP reinforcement and the surrounding concrete several techniques can be followed such as surface deformations, sand coating, over moulding a new surface on the bar or a combination of these techniques.

2.6.1.4 Shear Behaviour

Due to unreinforced resin layers between fibres, FRP bars are relatively weak in shear. The shear strength is usually governed by the relatively weak resin polymer and there is no reinforcement across the layers. Also the orientations of the fibres affect the shear strength too. In twisted or braided bars due to the variation of the orientation of the FRP bars, the shear strength is much stronger than in the straight bars [18].

2.6.2 Physical Properties

2.6.2.1 Density

FRP bars have a much lower density than steel and this property makes FRP bars easier to handle and transport.

Table 2.2 table shows typical densities of reinforcing bars.

Table 2.2: Typical Density of Reinforcing FRP Bars

Type of Bars	Steel*	GFRP*	CFRP*	AFRP*	BFRP**
Density (kg/m^3)	7900	(1200–2100)	(1500–1600)	(1250–1400)	1950

* Typical density of reinforcing bars (ACI 440.1R-03).

**Typical density of BFRP (www.magmatech.co.uk).

2.6.2.2 Coefficient of Thermal Expansion

In general, FRP materials have a lower thermal expansion coefficient compared to other metallic reinforcing materials. The coefficient of thermal expansion in FRP bars is quite variable in both the longitudinal and transverse directions. In the longitudinal direction the coefficient relies on the type of fibres and volume fraction of the fibre whereas in the transverse direction it relies on the type of resin. For instance, the strength of FRP fibre perpendicular to the fibre axis is ten times lower than the strength of a FRP fibre which is parallel to the longitudinal axis [21].

Different types of FRP have different values of thermal expansion coefficient as shown.

Table 2.: Typical Coefficients of Thermal Expansion for FRP Reinforcing Bars * (10^{-6}/C)

Direction	Steel*	GFRP*	CFRP*	AFRP*	BFRP**
Longitudinal, αL	11.7	(6.0–10.0)	(-9.0 –0)	(-6.0 – -2.0)	2 1/K
Transverse, αL	11.7	(21.0–23.0)	(74.0–104.0)	(60.0–80.0)	

*Typical coefficients of thermal expansion of reinforcing bars for fibre fraction ranging from 0.5 to 0.7.

** Typical coefficient of thermal expansion of BFRP bars (www.magmatech.co.uk).

2.6.2.3 Effect of High Temperature and Fire Resistance

According to ACI 440.1R-03 the use of FRP reinforcement bars is not desired in places which are vulnerable to fire accidents. Due to the high temperature the polymer will soften and this will cause the modulus of elasticity to reduce.

A major concern which is worth discussing here is when FRP materials are to be used in an environment with an elevated temperature. The tensile strength and elastic modulus of unidirectional FRP materials are unaffected by the increase of temperature, but the transverse and off axis properties are noticeably reduced as the temperature approaches the glass transaction temperature of the polymer matrix. The glass transaction temperature can be defined as a temperature in which the polymer matrix changes from a glass like state into a state which is similar to rubber. This will result in thermal softening and a significant reduction of strength and modulus will be observed. The change in structural stiffness properties after crossing the glass transaction temperature is very important because of the serviceability criteria that govern the design of FRP reinforced concrete sections [22].

Previous research carried out by Saafi [23], has shown that the concrete cover of the RC beam has the main influence on the response of FRP reinforced RC beams. Also he suggested that due to the rapid degradation of FRP bars under temperature, FRP reinforced RC beams exhibit significant degradation in shear and flexure resistance. Therefore, the minimum required cover for fire resistance in FRP RC beams is 64mm. whereas, the required cover for the same case in steel RC beams is 30mm.

Moreover, the components of FRP composite materials mainly consist of carbon, hydrogen and nitrogen atoms. These chemical materials are highly flammable and release dangerous toxic gases which are hazardous; therefore this has to be taken into consideration when using these materials in problems which are associated with fire resistance [24].

2.6.2.4 Thermal Conductivity

Thermal conductivity is the ability of a material to transfer the heat through it. In general the thermal conductivity of all FRP materials is very low, therefore they have very good heat insulation [24].

2.6.3 Long Term Behaviors

2.6.3.1 Creep Rupture

Under severe environmental conditions such as high temperature, ultra violet radiation exposure, high alkalinity, wetting and drying cycles, or freezing and thawing cycles, FRP reinforcement bars subjected to a static load will fail over a period of time. This is usually known as creep rupture or static fatigue which is not a big issue in the conventional steel reinforced concrete except in a very high temperature and fire conditions.

In general the glass fibres are the weakest fibres in creep rupture closely followed by aramid fibres. The least susceptible fibres to creep ruptures are carbon fibres (ACI 440.1R-03) and this behaviour is highly influenced by environmental factors such as temperature and moisture.

2.6.3.2 Durability

Many aspects influence durability of FRP reinforce RC elements, such as problems associated with the environmental degradation of the polymer matrix. The different types of polymer matrix in the composite are subjected to moisture absorption which results in the change of dimensions that eventually generate internal stresses. Another major factor that affects the performance of FRP materials is their susceptibility to ultra violet radiation exposure. This may result in loss of bond strength between the fibres and the matrix resulting in the ingress of moisture into the material. Past studies indicated that moisture may cause the acceleration of the static fatigue especially in glass fibre and this will cause the reduction of tensile strength and elastic modulus in response to moisture absorption [21].

2.7 Basalt Fibre Reinforced Polymer Rebar

Basalt is a natural and safe material; it is a type of igneous rock that solidifies from volcanic lava and can be found in many places around the world more than any other raw material. A third of the earth's crust consists of basalt, see Figure 2.12[20] .

Figure 2.12 Natural Basalt

Basalt rock has many advantages which make it desirable in the production of fibres that can be used for many purposes. The selection of the proper basalt rocks for manufacturing the basalt continuous fibres needs special knowledge, because not all the types of basalt rock are suitable for the production of basalt fibres, especially continuous basalt fibres. Only basalt rock that contain special chemicals as shown in Table 2.5, can be used to produce fibres to give a required strength, durability, elasticity, electric and heat insulation. Specialized companies such as BFCMTD and BF&CM, have practical experience in selecting the suitable basalt rocks for producing the basalt fibres.

Table below shows the chemical component of BFRB [10].

Table 2.5 Chemical Composition of BFRP

Element	**%**
SiO_2	58.7
Al_2O_3	17.2
Fe_2O_3	10.3
MgO	3.82
CaO	8.04

Na_2O	3.34
K_2O	0.82
TiO_2	1.16
P_2O_5	0.28
MnO	0.16
Cr_2O_3	0.06

Basalt can be extracted as a raw material very easily and cheaply by explosives of a quarry. Then the process of crushing the basalt rocks into small pieces (12.7mm) begins. It can be used as a crushed stones for many construction purposes such as embankments of railways, roads, and concrete fillings see below Figures.

Figure 2.13 Basalt Quarry

Figure 2.14 Crushed Basalt

To make basalt fibres, crushed basalt rocks are melted in a large furnace at about 1400-1700°C for 7 hours. After the melting process, the melted basalt will be passed through special fixture made from platinum and consists of set of regular holes. These fixtures are called bushing in the industry [25].

Fibres from basalt rock has a natural durability and high corrosion resistance in extreme environments, good electric, sound and heat insulation properties, and high resistance to chemical attack from substances such as acids, salts, alkalis which makes it useful for application in many various fields and industries.

The first attempt at producing basalt fibres goes back to 1923 in the United States. After World War II there were more investigations by research in the US, Europe and the Soviet Union especially for applications in aerospace and the military. The first production company was in Kiev-Ukraine in 1985, followed by the joint Ukraine-Japanese enterprise in 2000 [10].

Corrosion resistant basalt fibre rebar is a range of basalt fibre composite reinforcing bar for use in concrete, mortar and cast stone. It is a sensible replacement for stainless rebar for applications where corrosion, magnetic fields or electrical discharge could be a problem. The figure below shows basalt fibre rebars.

Basalt composite rebar is manufactured from continuous basalt filaments, epoxy and polyester resins using the pultrution process. It consists of 80 % basalt rock fibre by weight and the balance in epoxy, Dacron winding and sand [26].

Among all the available fibre reinforcement rebar, basalt fibre reinforced rebar BFRP currently is the most widely used in the USA, Canadian, Japanese, German and Italian markets [6], and this because of the high tensile strength of basalt bars which is twice of that glass fibres and has a 15-30% higher modulus of elasticity. Moreover, basalt fibres are more durable in an alkaline environment compared to glass fibres [6].

Figure 2.15 Basalt Fibre Rebar

Basalt reinforcing mesh is designed for reinforcing road and highway overlays to make the pavement more durable because it has low thermal expansion it can reduce the cracking that occurs with high temperatures on the roads and heavy traffic loading. Basalt reinforcing mesh makes it possible to reduce the thickness of the asphalt concrete pavement up to 20%.

Basalt composite rebar is non-magnetic and does not include magnetic field when exposed to electro-magnetic or radio-frequency energy. Hence it can be used in applications like a magnetic resonance imaging (MRI) room and around radio frequency identification equipment.

2.7.4 Applications

Basalt rebar can be used in the same way as conventional steel rebar. Some techniques need to be changed, these techniques include bending and cutting in the construction site but the basic processes are the same. Figures below show basalt rebar being used in construction.

Figure 2.16 Using basalt rods in construction sites

Basalt fibre reinforced polymer has been used in straight and curved form in the construction of Multimedia Fountain Park which is located in Podzamcze, Warsaw in November 2010 [4]. The corrosion resistant BFRP or RockBars were used instead of conventional steel rebar to increase the life span of the fountain and to reduce the cost of future maintenance.

Figure 2.17 Using BFRP as Internal Reinforcement in Poland

The Thompson Bridge project in Fermanagh, is a single span replacement bridge to carry the two-way A class road, which used BFRP or Rock-Bar as reinforcement of the bridge concrete slab deck in August 2010 [4].

Figure 2.18 Using BFRP as internal Reinforcement in Northern Ireland

Comparison of some characteristics of steel reinforcement and BFRP rebar shown in below table

Table 2.6: Comparison between Steel Bars and Basalt Bars [3]

Characteristics	**Steel**	**BFRP**	**Comments**
Density g/cm³	7.8	1.95	BFRP is 4 times lighter that steel rebar.
Weight of 1 linear meter, kg 10mm diameter 12mm diameter	 0.617 0.888	 0.15 0.221	
Ultimate strength N/mm² Tensile Compressive	 485 485	 1200 420	BFRP is 2 times stronger than steel.
Young's Modulus GPa	200	52-57	BFRP has 66 – 111 times less heat conductivity than and the expansion is 12 times.
Thermal conductivity coefficient	38	0.35-0.59	
Coefficient of linear thermal expansion 10^{-6} / °C	12	1.0	
Amount of 1 metric ton of rebar, linear meters 10 mm diameter 12 mm diameter	 1621 1126	 5848 4330	With BFRP we can transport 4 times more rebar than steel.
Percentage elongation	14.2	2.2	BFRP not suitable for quake zones.
Poisson's ratio	0.3	NA	

2.8 Design Philosophy

Design guidelines for FRP RC structures have been developed in Japan (JSCE, 1997), Canada (ISIS, 2001; CSA-S806, 2002), USA (ACI 440.1R-01, 2001; ACI 440.1R-03, 2003; ACI 440.1R-06, 2006), and Europe [27].

Table below illustrate historical development of the existing publications for guiding the design with FRP [28].

The recommendations governing the design of FRP RC structures currently available are mainly given in the form of modifications to existing steel RC codes of practice, which uses the limit state design approach. Such modification consists of basic principles, strongly influenced by the mechanical properties of FRP reinforcement, and empirical equations based on experimental investigations on FRP RC elements.

With respect to steel when dealing with FRP reinforcement the amount of reinforcement to be used has to be determined by a different approach, due to the lower stiffness and high strength of composite materials. In fact, for FRP reinforcement, the strength to stiffness ratio is an order of magnitude greater than that of steel by approximately %5, and this affects the distribution of stresses along the section.

Hence, when considering a balanced section, the neutral axis depth for FRP RC sections would be very close to the compressive side. This implies that for such a section, a larger amount of the cross section is subjected to tensile stresses and the compressive zone is subjected to a larger strain gradient. Hence, for similar cross sections to that of steel, much larger deflections and less shear strength are expected [29].

Table 2.7: Historical Development of the Existing Publications for Guiding the Design with FRP

1970s	**1996**	**1997**
Use of fibre reinforcement in concrete	The European Committee for Concrete (Eurocrete) published a set of design recommendations for FRP RC	The Japan Society of Civil Engineers (JSCE) published a set of design recommendations for FRP RC
1999	**2000**	**2001**
The Swedish National code	The Canadian Standard	The ISIS Canada published a

for FRP RC was published	Association (CSA) published a set of design recommendations for FRP RC bridges (CAN/CSA S6-00)	manual on the use of internal FRP reinforcement The American Concrete Institute (ACI 440) published the first version of design recommendations for internal FRP reinforcement (440-1R)
2002	**2003**	**2006**
The CSA published a set of design recommendations for FRP RC buildings (CAN/CSA S806-02) CUR Building & Infrastructure published a set of design recommendations for FRP RC (The Netherlands)	ACI Committee 440 published the second version of guidelines 440	The National Research Council (CNR) published the Italian design recommendations for internal FRP reinforcement (CNR-DT 203/2006) ACI Committee 440 published the third version of guidelines 440.1R

2.8.1 Review of Current Guidelines Design Philosophy

Current design guidelines and recommendations for structural concrete reinforced with FRP provide information on the use of common FRP materials such as glass (GFRP), aramid (AFRP) and carbon (CFRP). Up to now there is no design guidelines reported for basalt (BFRP).

Japan

Japan Society of Civil Engineers (JSCE) design guidelines are based on the modification of the Japanese steel RC code of practice, and can be applied for the design of concrete reinforced or pre-stressed with FRP rebar. The JSCE design philosophy reported both material and member safety factors to be slightly higher than the ones used for steel reinforcement. Although the flexural design covers both types of flexural failures, there is no information about the predominant mode of flexural failure that would result from the application of the proposed partial safety factors [30].

Europe

The European design guideline by the Eurocrete project [27] based on the modification of British (BS8110-1997) [31] and European RC codes of practice [32] . The guidelines include a set of partial safety factors for the material strength and stiffness that take into consideration both the short and long term structural behaviour of FRP reinforcement; and hence the adopted values are relatively high when compared with the values adopted by other guidelines. The guidelines do not make any distinction between the two types of flexural failure which are concrete rupture failure and FRP bar rupture failure. In addition they do not provide clear indications about the predominant failure mode which would result from the application of these partial safety factors.

Canada

The Canadian Standards Association (CSA) design guidelines CAN/CSA-S806-02 [33] are the most recently issued guidelines on the design and construction of building components with FRP. In addition to the design of concrete elements reinforced or prestressed with FRP, the guidelines also include information about characterization tests for internal FRP reinforcement. The guidelines were approved in 2004, as a national standard of Canada and it is intended to be used in conjunction with the national building code of Canada CSA A23.3 2004 [34].

The document prescribes that the factored resistance of a member, its cross section, and its connection shall be taken as the resistance calculated in accordance with the requirements and assumptions of this standard, multiplied by the appropriate material resistance factors. The factored member resistance shall be calculated using the factored resistance of the component materials with the application of an additional member resistance factor as appropriate [34].

As for the predominant mode of failure, the CSA S806-02 remarks that all FRP reinforced concrete sections shall be designed in such a way that failure of the section is initiated by crushing of the concrete in the compression zone [35].

The Canadian network of centre of excellence on intelligent sensing for innovative structures has also published a design manual that contains design provision for FRP RC structures (ISIS, 2001). The guidelines also provide information about the mechanical characteristics of commercially available FRP reinforcements. This guideline is also based on modifications to existing steel RC codes of practice, assuming that the predominant mode of failure is flexural, which would be sustained due to either concrete crushing (compressive failure) or rupture of the outermost layer of FRP reinforcement (tensile failure) .

USA

ACI Committee on Fibre Reinforced Polymer Reinforcement, Printed documents

- ACI 440.1R-6, **Guide for the Design and Construction of Structural Concrete Reinforced with FRP Bars** 2006.

- ACI 440.5-08, **Specification for Carbon and Glass Fibre Reinforced Polymer Reinforcing Bars.**
- ACI 440.2R-08, **Guide for the Design and Construction of Externally Bonded FRP Systems for Strengthening Concrete Structures.**
- ACI 440.4R, **Pressurising Concrete Structures with FRP Tendons.**
- ACI 440R-96, **State-of-the-Art Report on Fibre Reinforced Plastic (FRP) Reinforcement for Concrete Structures.**
- ACI 440.1R-03, **Guide and Construction of Concrete Reinforced with FRP Bars**.

The recently issued American guideline ACI 440.1 R-06 will be discussed in details within this thesis in the following section.

2.8.2 Limit State Flexure Design of FRP RC structures According to ACI code.

The design philosophy and methodology for concrete beams reinforced with FRP is similar to the design philosophy of conventional steel reinforcements with the consideration of the differences in the mechanical behaviour of the FRP bars. In the design of steel reinforced concrete structures is based on the linear elastic perfectly plastic behaviour of steel bars which provides enough ductility to the whole structure. Whereas FRP bars do not undergo plastic deformation therefore some modification is required.

The American Concrete Institute (ACI) design guidelines for FRP reinforced structural concrete (ACI 440.1R-06, 2006) are based on the modification of the (ACI 318-02, 2002) steel code of practice. The ACI 440 design guide is based on the fact that FRP behaviour is brittle. However; in the design of FRP reinforced concrete beam, both failure either FRP rupture or concrete crushing is acceptable in case that the strength and serviceability criteria are satisfied. To compensate for the lack of ductility in FRP reinforced concrete beams, the design guide suggests that the margin of safety must be higher than that used in conventional steel reinforced concrete design. [36].

Based on the previous research it has been accepted widely by the researchers that FRP is a brittle elastic material and behaves linearly up to failure without exhibiting any yielding. Therefore concrete crushing failure is more desirable for flexural members reinforced with FRP [37] as the concrete exhibits some plasticity before crushing. This will explain why the same resistance factor 0.9 for steel which ensures the ductile failure of under reinforced member cannot be used with the FRP reinforced members. The resistance factor for over reinforced FRP sections i.e. concrete crushing failure is given as 0.65, and 0.55 for under reinforced FRP section i.e. FRP tensile rupture which is brittle failure [38].

The design strength,f_{fu}, and design failure strain, ε_{fu}, are determined from the guaranteed strength and guaranteed failure strain by multiplying them by an environmental factor, C_E, which relies on the fibre type in the bar and the type of service intended, as shown in Table 2.8.

Table 2.8: The Environmental Reduction Factor for FRP Rebar from ACI 440.1R-06

Exposure Condition	**Fibre Type**	**Environmental Reduction Factor C_E**
Concrete not exposed to ground and weather	Carbon	1.0
	Glass	0.8
	Aramid	0.9
	Basalt	Not given
Concrete exposed to ground and weather	Carbon	0.9
	Glass	0.7
	Aramid	0.8
	Basalt	Not given

The reinforcement ratio and the balanced reinforcement ratio as per current ACI design guide can be given as:

$$p_f = \frac{A_f}{bd} \qquad (1)$$

Where, A_f is the area of reinforcement, b and d are the cross sectional dimension of the section.

$$p_{fb} = 0.85\beta_1 \frac{f'_c}{f_{fu}} \frac{E_f \varepsilon_{cu}}{E_f \varepsilon_{cu} + f_{fu}} \qquad (2)$$

Where, the β_1 factor depends on concrete strength, f'_c is the concrete strength from the tests, E_f is the guaranteed longitudinal modulus of elasticity of the FRP, ε_{cu} is the ultimate compressive strain in the concrete which is usually 0.0035 and f_{fu} is the guaranteed longitudinal tensile strength of the FRP bars.

In doubly reinforced FRP concrete sections if FRP bars are used as compression reinforcement, as per ACI code, the contribution of FRP to carry the compressive strength should be neglected. The flexural capacity of FRP reinforced concrete beams does not show any desirable or undesirable effects of FRP bars in the compression zone [5].

In the case of FRP reinforced concrete sections, the mode of failure for an under reinforced section will be governed by the rupture of FRP bars. Whereas the mode of failure of over reinforced concrete section will be by the crushing of concrete as in the case of steel reinforced concrete sections. The balanced reinforcement given in equation (2) above will ensure the rupture of FRP bars and the crushing of concrete to happen at the same time. This difference is very pivotal as in the case of FRP beam where both modes of failure are brittle owing to the linear elastic behaviour of the FRP bar. However the crushing of concrete in the compression zone can be regarded to be less brittle than the rupture of FRP bars in tension zone [5]. This will lead us to the conclusion that the FRP reinforced concrete beams are better to be designed as over reinforced in comparison to the steel beam which is preferred to be designed as under reinforced.

The nominal moment capacity for over reinforced FRP concrete section is given as:

$$M_n = A_f f_f \left(d - \frac{a}{2}\right) \qquad (3)$$

Where

$$a = \frac{A_f f_f}{0.85 {f'}_c b} \qquad (4)$$

And

$$f_f = \sqrt{\frac{(E_f \varepsilon_{cu})^2}{4} + \frac{0.85 \beta_1 {f'}_c}{p_f} E_f \varepsilon_{cu}} - 0.5 E_f \varepsilon_{cu} \qquad (5)$$

Here, f^f is the stress in the FRP rebar at concrete compressive failure, a is the depth of the stress block, d is the effective depth of the section; b is the width of the beam and A_f is the area of FRP reinforcement. E_f is the longitudinal modulus of elasticity of the FRP bar, p_f is the reinforcement ratio and ε_{cu} is the maximum compressive strain in concrete.

The preference of the concrete crushing to the FRP rupture is also attributed to the fact that the confined concrete can provide some post-peak large strain capacity, even at reduced stress levels [5]. The linear elastic behaviour of FRP bars also does not allow the formation of plastic hinges and so moment redistribution cannot be applied. Where FRP bars are used in layers, the stress in each layer should be calculated separately to calculate the moment capacity of the section in contrast to the steel bars, where it is allowed to assume that the resultant tensile force in the bars acts through the centroid of the bar layers. This has also been verified by the various researchers that the anisotropic nature of the material does not significantly affect the flexure behaviour of the section [37].

Sections with smaller amounts of reinforcement than the balanced ratio fail by the rupture of the FRP in the tension zone, while sections with larger amounts of reinforcement fail by the concrete crushing in the compression zone. The minimum reinforcement area can be found from Equation 6, which has been determined by multiplying the current ACI 318-05 equation of minimum required reinforcement for steel by 1.64 to prevent failure upon concrete cracking.

$$A_{f,min} = \frac{4.9\sqrt{f'_c}}{f_{fu}} b_w d \geq \frac{330}{f_{fu}} b_w d \qquad (6)$$

As recommended in the ACI 40 code for the design of FRP reinforced concrete structures, the design procedure based on the limit state design principles that the member designed for the required strength should then be checked for fatigue endurance, creep rupture endurance and the serviceability criteria [36]. The serviceability criteria, primarily deflection and crack width, are fundamental issues that govern the design of FRP reinforced concrete structures. The high tensile strength and low modulus of the FRP material mean that the reinforced member is highly susceptible to deformation. Due to the lower stiffness of FRP bars compared to steel bars, the members reinforced with FRP bars exhibits noticable deflection and larger crack widths than the members reinforced with conventional steel bars. Because of the linear elastic brittle behaviour of FRP bars, the ACI code does not allow the use of moment redistribution because plastic hinges cannot form.

2.8.3 Serviceability

Because of the lower modulus of elasticity of the FRP bars compared to steel bars for the same reinforcement ratio, the FRP reinforced beams exhibits larger deflections than steel reinforced beams. As a result extensive cracking along the length of the beam will occur consequently reducing its flexural stiffness and resulting in more deflection.

The serviceability limit state design for FRP reinforced concrete beams considers two important serviceability conditions which are deflection and cracking.

2.8.3.1 Cracking

Even though the stress-strain relationship is very important for the determination of the bending moment strength of the FRP reinforced concrete beam, the stiffness behaviour may be equally important for various other structural requirements. This may be particularly important for dictating the various serviceability criteria. The stiffness or longitudinal modulus of elasticity of the FRP bars is significantly lower than the steel bars. This may cause an excessive deflection of the beam and hence larger crack widths will occur. Due to low modulus, the FRP material is highly susceptible to the condition of high deformation such that serviceability criteria can be a fundamental issue on the design of FRP reinforced concrete beams.

On the basis of the research carried out by Nanni [39] for a comparison study between the flexure behaviour of aramid FRP reinforced beams and conventional steel reinforced concrete beams, some important principles can be stated. The moment curvature analysis for both steel reinforced and AFRP reinforced beams was performed. This identified that the FRP reinforced sections exhibits the same maximum moment and curvature as in the case of steel reinforced concrete beams with a slightly smaller reinforcement ratio, however, the flexural rigidity of the FRP section is only 38% that of the steel reinforced beam. This will lead us to the fact that the deflection criteria may be as important as the flexural strength in the case of FRP reinforced beams [37].

The maximum crack width in accordance with ACI 440.1R-21 can be calculated as the following equation:

$$w = 2\frac{f_f}{E_f}\beta k_b\sqrt{{d_c}^2 + \left(\frac{s}{2}\right)^2} \qquad (7)$$

In which w is maximum crack width, f_f is the stress of the reinforcement, E_f is elastic modulus of the reinforcement, β is a ratio of distance between neutral axis and tension face to distance between neutral axis and centroid of reinforcement, d_c is the concrete cover thickness, s is bar spacing and k_b is the coefficient of the degree of the bond between FRP bars and the surrounding concrete.

Because the corrosion resistance property of FRP bars under extreme environment conditions the permissible crack width is greater than of steel, the ACI code allows the permissible crack width to be 0.020 in (0.5 mm) for exterior exposure conditions, and 0.028 (0.7 mm) in for interior conditions. Whereas in steel reinforced concrete it is 0.013 in (0.3 mm) for exterior conditions and 0.016 in (0.4 mm) in interior conditions.

2.8.3.2 Deflection

Traditionally deflection has been computed with an elastic deflection equation that includes an effective moment of inertia (I_e) which was originally introduced by Branson for steel reinforced concrete [40]. Past studies indicated that using Branson's equations gives a response that is too stiff for FRP reinforced concrete and underestimates the deflection as a result [41]. The reasons for this have been attributed to a number of different factors including poor bond and excessive cracking; both were thought to be responsible for a loss of tension stiffening with FRP reinforcement. Therefore the applicability of the Branson equation for FRP reinforced concrete beams can be questioned.

Branson's equation was originally developed for steel reinforced concrete and it uses an effective moment of inertia I_e to compute deflection in conjunction with elastic deflection formulas. This relationship was empirically derived and represents a gradual transition from the gross (uncracked) moment of inertia I_g to the cracked moment of inertia I_{cr}. In the generalized form this can be expressed as:

$$I_e = \left(\frac{M_{cr}}{M_a}\right)^m I_g + \left[1 - \left(\frac{M_{cr}}{M_a}\right)^m\right] I_{cr} \leq I_g \qquad (12)$$

Where, for the steel reinforced beam, the exponent m is found to be equal to 3. However the cubic term is based on the concept of average effective moment of inertia and an exponent of 4 was found to give better approximations of effective moment of inertia for individual sections [42]. Branson's equation was confirmed for the ratios of gross moment of inertia I_g

and cracking moment of inertia I_{cr} between 1.5 and 4 [43]. FRP reinforced concrete beams generally have values of this ratio greater than 5 (usually between 5 to 25), thus leading to a much stiffer response and under-prediction of computed deflections when used in conjunction with the original Branson equation [44]. The exponent m has also physical importance in the sense that it provides a smooth transition from the gross moment of inertia to the cracking moment of inertia as the load reaches the ultimate value. Hence it can be concluded that the transition from the gross moment of inertia of FRP reinforced beam to the cracking moment of inertia is faster, which explains the faster reduction in the stiffness of the beam. However they are not completely amendable to the original Branson equation, which predicts relatively slower degradation with the exponent equalling 3. A suggestion of the “m” exponent to be greater than 3 is made by Dolan. In the case of GFRP reinforced beams with the reinforcement ratio less than 4%, they can have a ratio of the un-cracked to cracked moment of inertia of between 5-16 and this demonstrates the importance of the exponent “m”.

In the case of FRP reinforced concrete beams where the experimental deflection exceeds the moment of inertia of cracked section (I_{cr}) limitation on deflection, there may not be enough bond between the FRP bars and the surrounding concrete. Thus the Branson equation can provide the transition from gross moment of inertia (I_G) to the cracked moment of inertia (I_{cr}). In 1997, Therialut [42] proposed such a modification as follows:

$$I_e = \alpha I_{cr} + \left(\frac{I_g}{\beta} - \alpha I_{cr}\right)\left[\frac{M_{cr}}{M_a}\right]^3 \qquad (13)$$

Where α and β are equal to 0.87 and 7 respectively. In the above equation the factor α allows for the transition from the gross moment of inertia to the cracked moment of inertia.

The ACI committee 440.1R-03 [18] recommended a modification on the original Branson equation to reduce the tension stiffening component which depends on the ratio of gross to cracked moment of inertia to realistic levels. This relation was defined as:

$$I_e = \left(\frac{M_{cr}}{M_a}\right)^3 \beta_d I_g + \left[1 - \left(\frac{M_{cr}}{M_a}\right)^3\right] I_{cr} \leq I_g \qquad (14)$$

Where E_f and E_s are elastic modulus values for FRP and steel bars, the coefficient β_d was initially set equal to 0.6 and later defined as $\beta_d = \alpha_b\left[E_f/E_s + 1\right]$, and α_b is the bond dependent factor which assumed equal to 0.5 until more data became available and set $\alpha_b = 0.064(\rho/\rho_b) + 0.13$. Recent changes by ACI 440.1R-06 recommend using $\alpha_b = 0.2(\rho/\rho_b)$ .Nwys reported that the deflection prediction varies with the quantity of reinforcement [41]. He recorded also that the under-estimation of the deflection varies inversely with the reinforcement ratio. Sunna carried out tests on FRP reinforced concrete beams and reported similar results [45].

The deflection calculation based on the original or modified form seems to over-estimate the stiffness of the member hence resulting in under-predicting deflection. However, the predictions improve as the reinforcement ratio increases, and he proposed the following relationship:

$$I_e = \alpha I_{cr} + \left(\beta I_g - \alpha I_{cr}\right)\left[\frac{M_{cr}}{M_a}\right]^3 \qquad (15)$$

Where $\beta = 0.1e^{330\left(\rho E_f/E_s\right)^{1.2}}$ (16)

Where the value of α proposed to be between 0.85, 0.9 and 1 for GFRP, CFRP and steel reinforced concrete beams, respectively, with the respect to bond characteristic of the different materials.

Similar conclusions were made by Rafi relating to the over-prediction of the stiffness of the CFRP reinforced concrete beams [46]. In the past extensive studies have been conducted by previous researchers and a plot has been generated to illustrate the relationship between the reinforcement ratio and the discrepancy in theoretical prediction calculated by the Branson equation and actual deflection is shown in below figure [47].

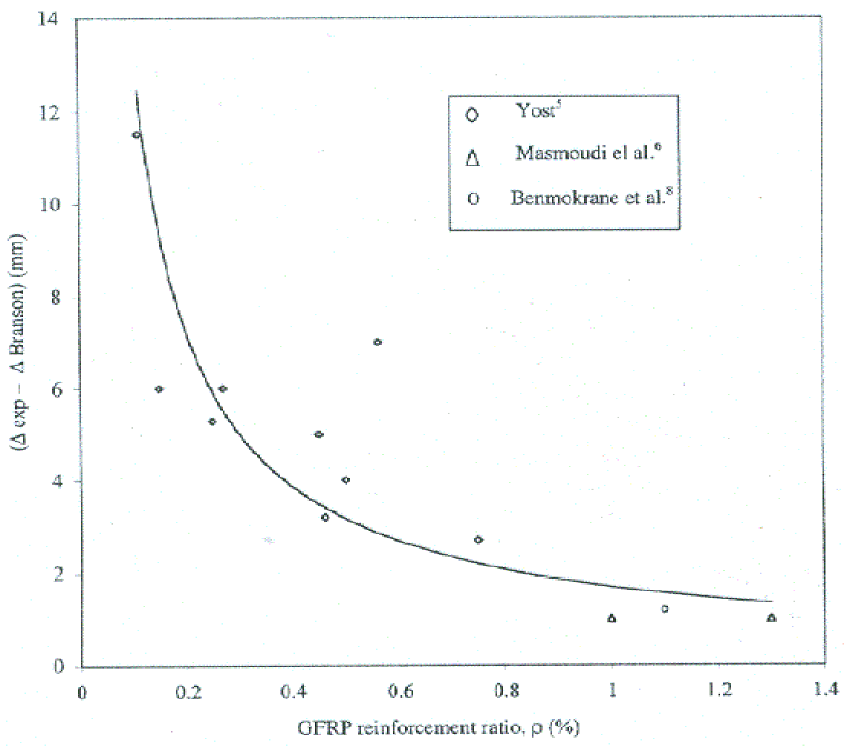

Figure 2.19 Effect of Reinforcement Ratio on the Deflection

In the above plot from the work done by Yost, Masmoudli and Benmokrane on the GFRP reinforced concrete beams it can be observed that when the lower reinforcement ratio has been used the discrepancy between the actual and theoretical deflection is higher, whereas this discrepancy is getting better with the increasing of the reinforcement ratio. From this we can suggest that the behaviour of FRP reinforcement concrete beams is completely different than the behaviour of steel reinforcement concrete beams. As a result tension stiffening plays a major role in the analysis of FRP reinforced concrete sections.

Previous research indicates that the ratio of gross moment of inertia to cracked moment of inertia in the case of GFRP reinforced concrete beams varies between 5 to 25 when the reinforcement ratio is between 2 to 3 [43]. Thus the working range of the Branson equations is for the cases when the reinforcement ratio used is less than 4%. In other words a reinforcement ratio of at least 3% is required in GFRP reinforced concrete beams to be within the working range of the Branson equation. To deal with this issue, Bischoff developed a theoretical model based on the actual mechanics of the structure including tension stiffening.

This model can generalize the relationship between all the parameters based on the fundamental mechanics of the structure and appropriate assumptions.

Bischoff gives the general formulation of the effective moment of inertia as follows [44]:

$$I_e = \frac{I_{cr}}{1-\varkappa_{ts}\eta\left({M_{cr}}/{M_a}\right)} = \frac{I_{cr}}{1-\eta\left({M_{cr}}/{M_a}\right)^2} \leq I_g \qquad (17)$$

Where:

$$\eta = 1 - {I_{cr}}/{I_g} \qquad (18)$$

And:

$$\varkappa_{ts} = {M_{cr}}/{M_a} \qquad (19)$$

The equation provided by Bischoff indicates that the tension stiffening factor $\varkappa_{ts}$ is similar to the approximation made for axial tension members and is based on the assumption that the tension stiffening strain varies inversely with the reinforcement stress at the crack location. That is, $\varkappa_{ts} \sim f_{b,cr}/f_b$. Where, $f_{b,cr}$ is the stress in the bar at first cracking and f_b is the stress in the bar at M_a . Therefore in the case of FRP reinforced beams with lower reinforcement ratio the tension stiffening strain is larger.

As discussed above, the stiffness of a FRP reinforced concrete section is a function of the reinforcement ratio. In the past many efforts have been made by researchers to understand this factor. In 2000, Toutanji and Safi indicated the effect of this factor on the exponent “m” in the original Branson equation. Similarly, Dolan suggested the limit of exponent “m” for FRP reinforced concrete beams as follows [47]:

For $\frac{E_{FRP}}{E_S}\rho_{FRP} < 0.3$ $\qquad m = 6 - \frac{10E_{FRP}}{E_S}\rho_{FRP}$

For $\frac{E_{FRP}}{E_S}\rho_{FRP} \geq 0.3$ $\qquad m = 3$

Where, E_{FRP} is the elastic modulus of GFRP bars used in the study, E_S is the elastic modulus of steel and ρ_{FRP} is the FRP longitudinal reinforcement ratio.

Based on other studies on the analysis of deflection of CFRP reinforced concrete beams, in 2005, Maji and Oronzco developed the following modification for effective moment of inertia [48]:

$$I_e = \gamma \left[\eta \left({}^{M_{cr}}/_{M_a} \right)^3 I_g + \left[1 - {}^{M_{cr}}/_{M_a} \right]^3 I_{cr} \right] \qquad (20)$$

Where γ is the modification factor and its value is equal to the ratio of elastic modulus of FRP to the elastic modulus of steel. ꞃ is a factor that depends on the reinforcement ratio (ρ) and it is given as:

$$\eta = 100\rho - 0.2 \qquad (21)$$

From the previous study on the analysis of deflection of FRP reinforced concrete beams it can be concluded that the deflection of FRP reinforced concrete beams is dependent on the reinforcement ratio and are affected by its lower modulus of elasticity.

According to the latest ACI 440.1R-06, in the case of a FRP reinforced concrete section a modified form of Branson equation is used to calculate the effective second moment of the beam as given in the following equation.

$$I_e = \left(\frac{M_{cr}}{M_a}\right)^3 \beta_d I_g + \left[1 - \left(\frac{M_{cr}}{M_a}\right)^3\right] I_{cr} \leq I_g \qquad (22)$$

Where, M_{cr} is the moment of cracking and β_d is a reduction coefficient for FRP reinforced beams and given as:

$$\beta_d = \frac{1}{5}\left(\frac{\rho_f}{\rho_{fb}}\right) \leq 1 \qquad (23)$$

In a similar way for a steel reinforced concrete section, the cracked second moment of area is given as

$$I_{cr} = \frac{bd^3}{3} k^3 + \eta_f A_f d^2 (1-k)^2 \qquad (24)$$

Where $k = c/d$ and it is the ratio of the depth of the neutral axis to the effective depth of the section under service load and η_f is the modular ratio for the FRP reinforcement.

3. Test Programme

This section describes the materials that were used for the investigation of the flexural behaviour of two BFRP reinforced concrete beams. The behaviour of BFRP RC beams were compared to the behaviour of conventional steel RC beams. This section gives a comprehensive overview of the various materials that were used, their relevant characteristics, specifications and their associated properties.

3.1 Materials

The first objective is to investigate the flexure behaviour of BFRP RC beams and compare to the behaviour of conventional steel RC beams. The materials used were conventional concrete, steel bars and BFRP bars provided by MagmaTech.

3.1.1 Coarse Aggregate

The coarse aggregate used in this study was limestone with the maximum size of 20mm. The aggregates were angular (crushed) and free from clay and other impurities.

3.1.2 Fine aggregate

The fine aggregate was the grade “M” concreting sand purchased from a local supplier. The sand was free from clay and other impurities.

3.1.3 Cement

The cement provided by local supplier was 52.5 Cement CEM1.

3.1.4 Steel Stirrups and Compression Bars

For shear and compression reinforcement, the BFRP reinforced concrete beams were reinforced with 6.5mm mild steel.

3.1.5 Steel Bars

For reinforcing the two control steel reinforced concrete beams, 8mm diameter steel bars were used. The bars were ordered from the local steel supplier. The ultimate tensile strength obtained from the manufacturer was 650 MPa.

3.1.6 BFRP Bars

The BFRP bars used in this study were provided by MagmaTech and the nominal diameter was 8mm. The technical data for the BFRP bars and the actual cross-sectional area and the tensile strength of BFRP bars were taken from a study that has been undertaken by the University of Sheffield [49].

The average of actual cross sectional area for five samples of 8mm BFRP bars were calculated to be 46.982mm^2, mean Tensile Strength was 1465MPa, guaranteed tensile Strength was 1350MPa, Elastic Modulus was 47.5GPa and the Failure Strain was 0.030863, see below figure.

Figure 3.1 Basalt FRP Bars Used in Beams

3.2 Concrete Mix

A quantity of 72 litres of concrete mix has been used to test each of the BFRP RC beams. The BFRP reinforced concrete beams are referenced as BFRP RC1 and BFRP RC2. The mix proportion was the same for both beams, see Table 3.1.

Table 3.1: Mix proportions

Mix Content	**kg/m^3**
Cement	356
Gravel	1487
Sand	647
Water	193
Total	2683

Table 3.2: Number of specimens

Specimens	**Volume (l)**	**Number of Sample**	**Total volume (l)**
100mm cube	1	6	6
Beam	60	1	60

3.3 Equipment

3.3.1 Testing Machine

The testing machine used for this research was a Zwick 300kN capacity compression testing machine, as shown in below figure. The deflection was measured using a LVDT.

Figure 3.3 Zwick Testing Machine

3.3.3 Compression machine

A Toni-pact compression machine was then used to crush the concrete cubes as shown in below figure.

Figure 3.4 Toni-Pact Compression Machine

3.4 Test Procedure

This section includes a comprehensive description of the test procedures adopted for the flexural testing of the Basalt FRP reinforced beams. The test procedure includes the systematic summary of all activities involved with the test of the FRP reinforced beams. The test procedure primarily comprises the preparation of the cage, then mixing and casting of the beams followed by their testing. The whole experimental programme consisted of two basalt FRP reinforced concrete beams with the same reinforcement ratio, geometry and concrete strength of steel reinforced concrete beams. All reinforced concrete beams were (200x150x2000) mm.

3.4.1 Preparation of Cages

The reinforcement cage included the arrangement of the reinforcing bars and shear stirrups. The reinforcing bars were supported between the two points at the end of the beams as illustrated in the figure below. The spacing between the shear stirrups was set to be 120mm and tied to the main reinforcement by using mild steel tie wire.

Figure 3.5 the Cage of BFRP Reinforcement

3.4.2 Mixing and Casting of Beams and Cubes

Casting of the beams and cubes was one of the most important steps. This step was carefully undertaken to ensure the production of good concrete. The internal sides of the wooden formworks had form oil applied to ensure that the concrete doesn't stick with formwork as shown. The needle vibrator was used while casting the beams BFRP RC1 and BFRP RC2 to ensure there was enough compaction. Six concrete cubes were also cast of the same concrete for the determination of the compressive strength of the concrete for each beam as shown in the figure. The top surface of the cast beams was finished with a steel float in order to provide the smooth surface for the application of the load. The beams were then covered with saturated hessian.

The beams were then left for three days to set. After 72 hours, the beams were demoulded. The hessian covers were regularly sprayed with water so as to provide a regular supply of moisture. The cubes were kept in a curing tank under water at 20°C which provided the 100% humidity.

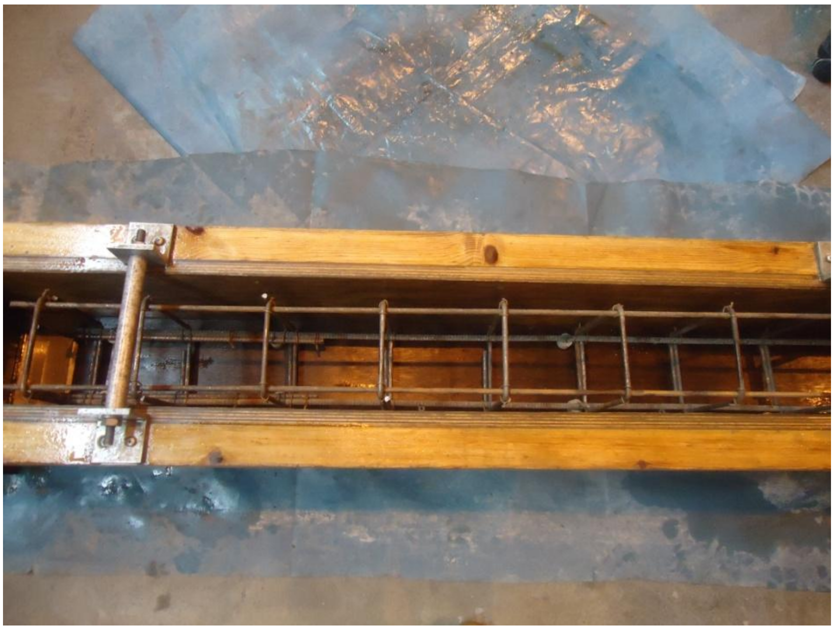

Figure 3.6 Formwork

Figure 3.7 Cast Beam and Cubes

3.4.3 Testing Beams

In this research, two FRP beams were tested and the results were compared to conventional concrete beams reinforced with steel bars. The concrete beams were tested as a part of undergraduate studies at the University of Liverpool.

The beams were positioned under the testing machine and roller supports were provided. Both supports were positioned at a distance of 100mm from the ends such that the effective span of the beams was 1800mm. The beam dimensions and loading configuration is shown in the figures below the experimental layout is show in Figure 3.9.

The beams were tested on Zwick testing machine in the university's concrete laboratory. This testing machine has a capacity of 30 tonnes.

The FRP reinforced concrete beams were fixed in place on a test rig with four points loading. This is achieved by applying the total load at two points spaced 600mm apart. A digital gauge was attached to measure the vertical deflection (mm) of the beam. The loading was controlled mechanically.

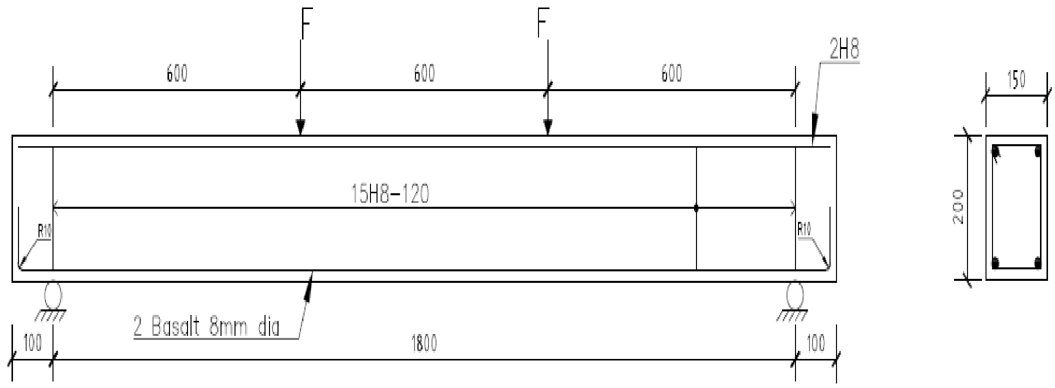

Figure 3.8 Diagrams of the BFRP RC Beam Dimensions and Loading Pattern

Figure 3.9 Experimental Layouts of the BFRP RC Beams

For the first part of the experiment, the load was applied at 0.5kN loading increments up to a load of 15kN. The deflection and load were recorded at each increment manually. The values of the load corresponding with the formation of the first observable hairline cracks were noted and were outlined in pencil on the beams, see Figure 3.10.

Figure 3.10 Markings of Outlines of Cracks and Their Loads on BFRP RC Beams

Then the load was set back to 0kN and increased at 0.5kN increments until collapse.
During the test, the deflection gauge for the second beam was detached at a load of 40 kN. Therefore, deflection measurements were not recorded beyond this load.

After the formation of major cracks as shown in Figure 3.11, deflection measurements were not stable. Furthermore, FRP has a very high tensile strength. This result in a higher deflection before failures occurs.

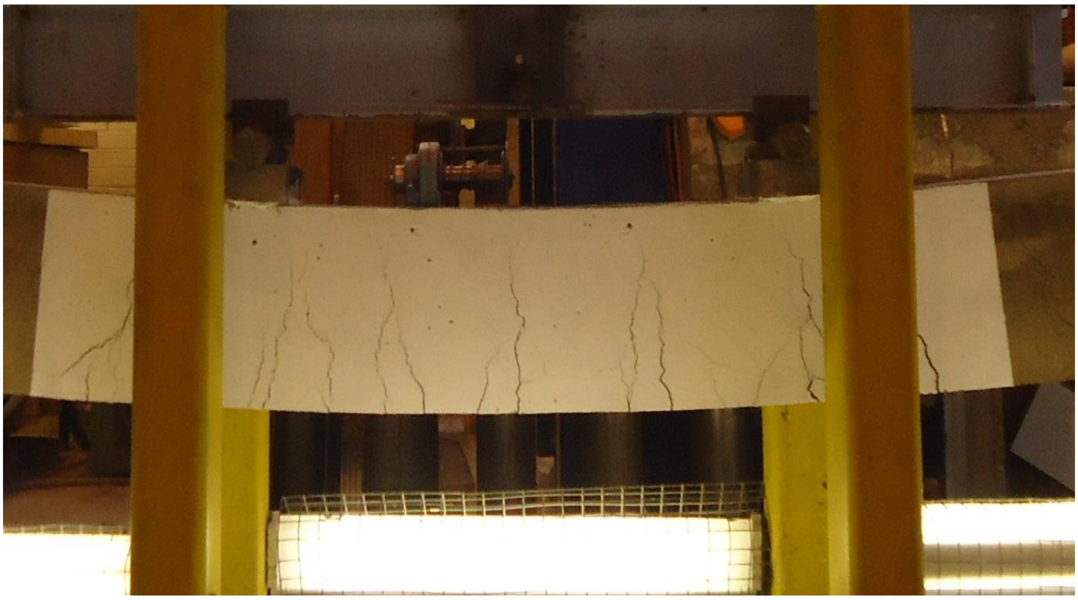

Figure 3.11 Formations of Major Cracks

3.4.4 Compression Tests of Cubes

Three sample cubes of the concrete used for each beam were tested. They had standard dimensions of (100x100x100) mm according to standard procedure BS 1881-127:1990 as shown in. The cubes were taken out of the moulds after 72 hours and placed in a curing tank with the same heat and humidity conditions as the beams to correspond to their concrete strength for seven days. The densities of the cubes were measured and calculated.

Figure 3.12 Casting Concrete Cubes for Compression Tes

Figure 3.13 Curing Concrete Cubes in the Tank

A Toni-pact compression testing machine was then used to crush the concrete cubes, with the load required to crush the cubes displayed on a digital readout. From these values, the strength of the concrete samples could be calculated, and an average value taken to determine the characteristic compressive strength of the concrete. The experimental layout is shown in the figure below. And the compressive strength details for concrete cubes shown in below table.

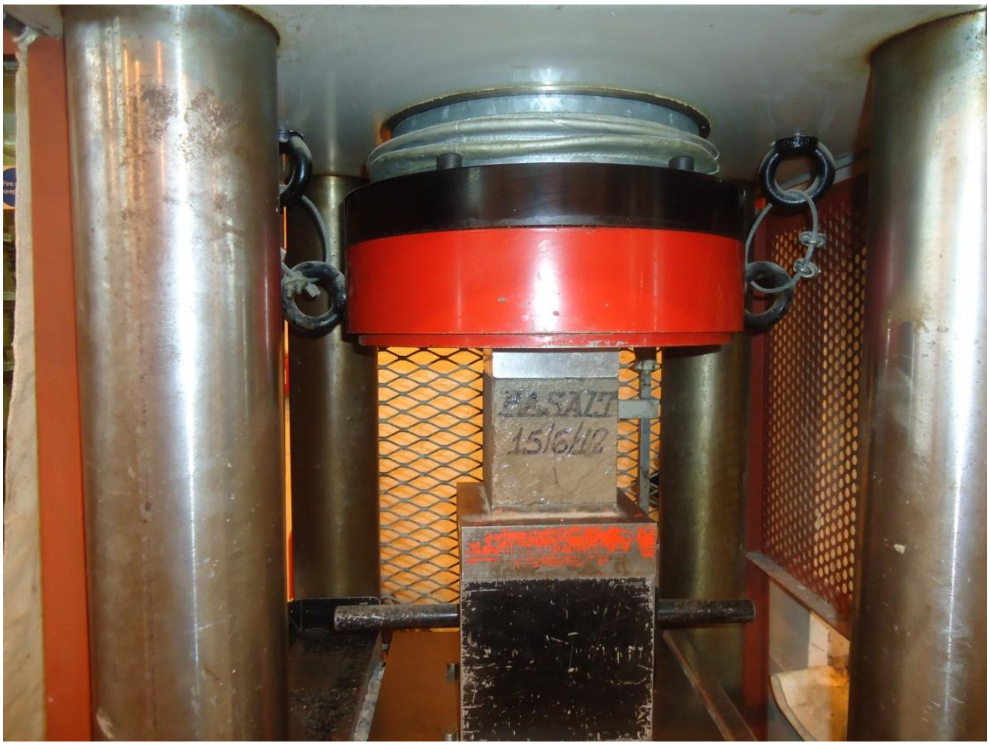

Figure 3.14 Toni-pact Compression Machine Used to Crush Concrete Cubes

Table 3.1: Compressive Strength Details for Concrete Cubes for BFRP RC Beams

Beam	***BFRP RC1***			***BFRP RC2***		
Cubes	***Density (kg/m^3)***	***Load (kN)***	***fc'(MPa)***	***Density (kg/m^3)***	***Load (kN)***	***fc'(MPa)***
1	2463	365	36.5	2460	453	45.3
2	2448	343	34.3	2444	459	45.9
3	2427	349	34.9	2456	478	47.8
Average	2446	352	35.2	2453	463	46.3

4 Finite Element Analysis

4.1 General

In the past years there have been many different methods used to study the structural response of concrete. Experiments have been widely used to study and analyse different members of concrete structures and their response under loading. This method is more accurate but it is extremely time consuming and the use of materials can be very costly. Finite element analysis has been used to study the response of these structures. Many attempts have been used in using the finite element analysis but unfortunately many early attempts to carry out this type of analysis was also very time consuming and costly.

In recent years many finite element analysis packages has been developed and it has now become the choice method to analyse concrete structures. The use of these packages is now much cost effective.

The finite element method (FEM) was first used in the 1950's, and has been continuously developed since then and now it is an important and powerful tool in solving engineering problems. The FEM shows detailed visualisation of where structures deform, and can indicate the distribution of stress, strain and displacement accurately.

4.2 Crack Model for Concrete

The process of forming cracks in concrete can be divided into three stages as shown in below figure.

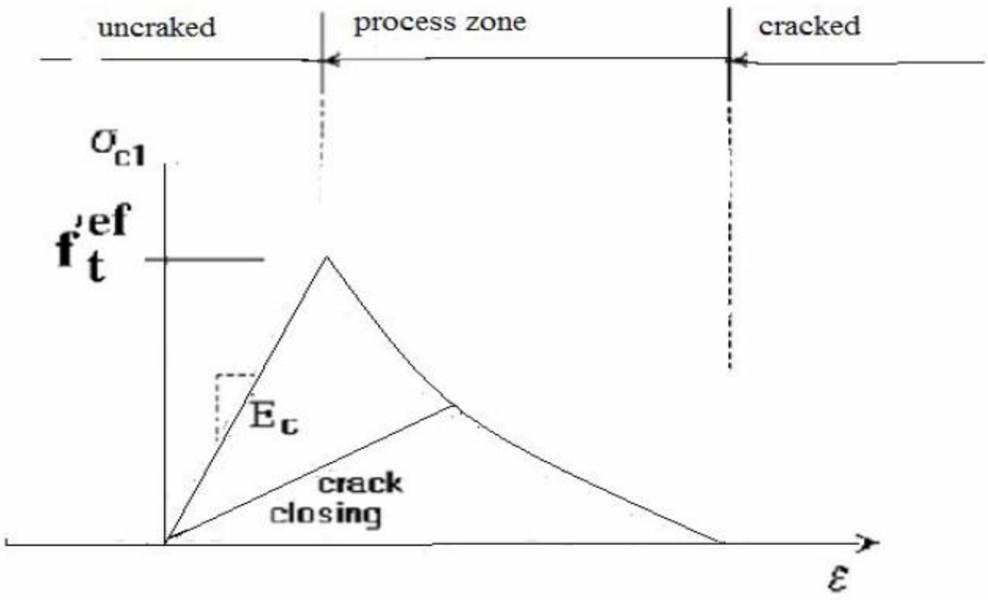

Figure 4.1 Stages of Crack Opening

The un-cracked stage, because concrete is considered to be a brittle material and its stress - strain relation in the un-cracked state in the direction of principal tensile strain is assumed linear up to the tensile strength. The crack formation takes place in the process zone with decreasing tensile stress on a crack face due to a bridging effect. Finally, after a complete release of the stress, the crack opening continues without the stress.

The tension failure of concrete is characterized by a gradual growth of cracks, which join together and eventually disconnect larger parts of the structure. It is usually assumed that the cracking formation is a brittle process and that the strength in the tensile loading direction abruptly goes to zero after cracks have formed. Therefore, the formation of cracks is undoubtedly one of the most important non-linear phenomena, which governs the behaviour of concrete structures.

Extensive research has been carried out on the numerical modelling of concrete cracking [50-52]. Concrete cracking may be modelled using either the concrete damage plasticity or the smeared crack model.

In this study the Concrete Damage Plasticity model has been used to model the cracking in concrete combined with crack band theory.

4.2.1 Concrete Damage Plasticity Model

The concrete damage plasticity model in Abaqus uses the concept of isotropic damaged elasticity in combination with isotropic tensile and compressive plasticity to represent the inelastic behaviour of concrete [53].

The evolution of the yield surface is controlled by two hardening variables, the tensile equivalent plastic strain ${\varepsilon_t}^{pl}$ and the compression equivalent plastic strain ${\varepsilon_c}^{pl}$ which are linked to the failure mechanisms under tension and compression loading.

In uniaxial tension, the stress-strain response follows a linear elastic relationship until it reaches the value of the failure stress σ_{t0}. After reaching the failure stress, the micro-cracks occur which is characterized by the softening stress-strain response Figure 4.2.a. In the case of uniaxial compression, the stress-strain relation is linear until reaching the initial yield point σ_{c0}, which is followed by stress hardening until the ultimate stress σ_{cu}, after which stress softening occurs Figure 4.2.b.

The concrete damage model in Abaqus is defined by using the concrete damaged plasticity, concrete tension stiffening, and concrete compression hardening options and, optionally, the concrete tension damage and concrete compression damage options.

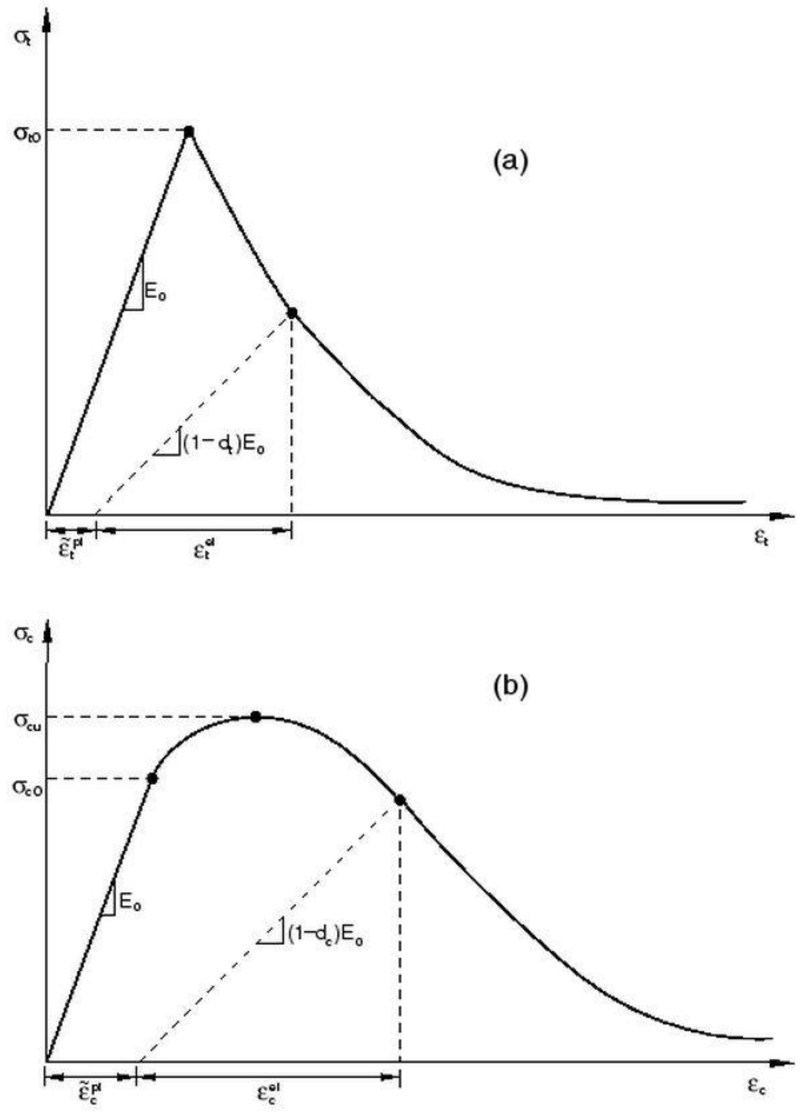

Figure 4.2 Response of Concrete to Uniaxial Loading in Tension (a) and Compression (b) [53]

4.3 FE Modelling of Reinforcement

For modelling reinforced concrete using the finite element method, there are three strategies available for modelling reinforcement bars [54-56]. These methods are the discrete model, the embedded model and the smeared model.

4.3.3 Discrete Model

In the discrete model, the reinforcement is modelled by either using a bar or beam element which is connected to the concrete mesh nodes. Therefore; there are shared nodes between both concrete and reinforcement elements. Furthermore, in the discrete technique the reinforcement is superimposed in the concrete mesh. As results, concrete exists in the same regions occupied by the reinforcement, see Figure 4.3.

The drawback of using the discrete model is that the concrete mesh is restricted by the location of the reinforcement.

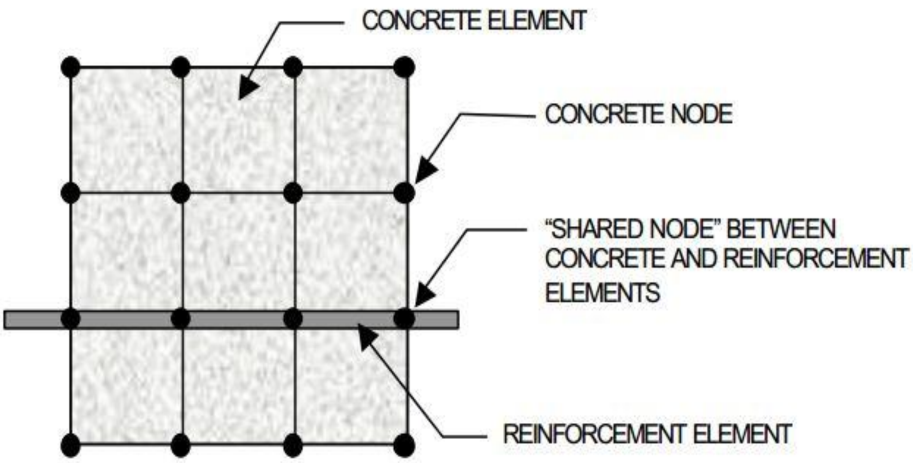

Figure 4.3 Shared Nodes Between Concrete Elements and Reinforcement Elements

4.3.4 Smeared Model

The smeared model assumes that the reinforcement is distributed uniformly in the concrete elements in a defined region of the FE mesh. As a result, the properties of the material model in the element are constructed from individual properties of concrete and reinforcement using composite theory. This method is useful for large scale models where the reinforcement does not significantly contribute to the overall response of the structure, see Figure 4.4.

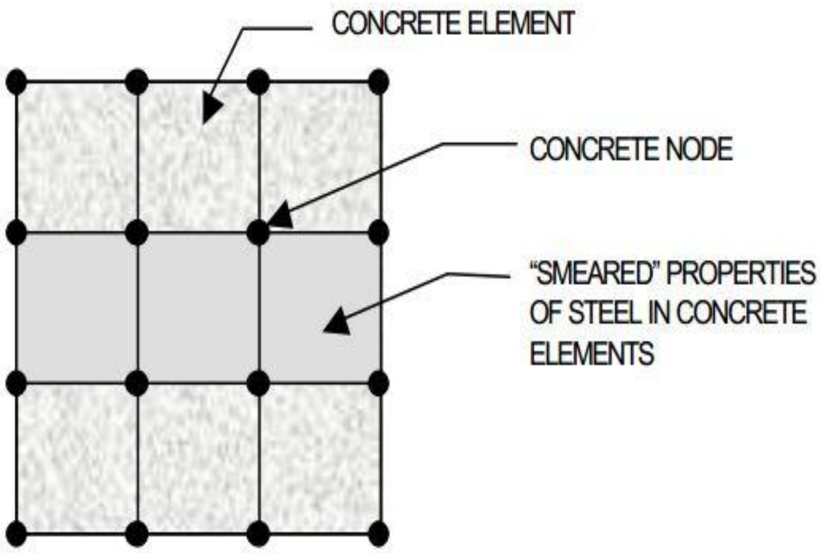

Figure 4.4 Smeared Formulations for Reinforced Concrete

4.3.5 Embedded Model

In this study the embedded method has been used to model the reinforcement in the reinforced concrete beams. The embedded method overcomes the drawback of mesh restrictions in the discrete and smeared methods, because the evaluation of stiffness in reinforcement elements will be carried out separately from the concrete elements. Moreover the displacement of reinforcement elements will be compatible with the displacement of surrounding concrete elements. The embedded method is very useful when used in complex models. However, this model increases the number of nodes and the degrees of freedom in the model; as a result, it requires more run time and increases the computational cost, see Figure 4.5.

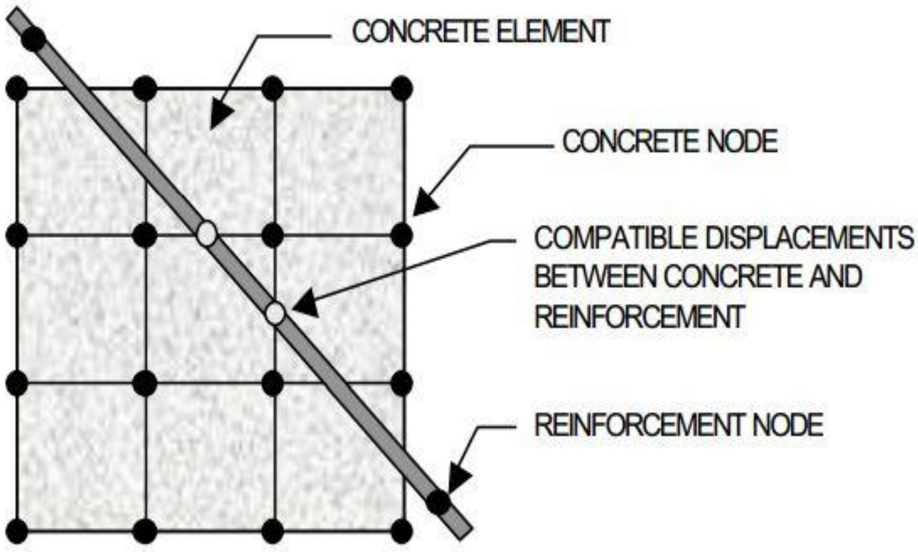

Figure 4.5 Embedded Formulations for Reinforced Concrete

4.4 Element Types

Abaqus has an extensive element library to provide a powerful set of tools for solving many different problems. Each element in Abaqus has a unique name, such as T2D2, S4R, C3D8I, or C3D8R. The element name identifies each of the five aspects of an element.

4.4.1 Concrete

3D and 2D models have been used for modelling plane, steel reinforced and BFRP reinforced concrete beams. In the 2D models, a four node quadrilateral plane stress element (CPS4R) was used to model the concrete. The element has four nodes with two degrees of freedom at each node, translation in the x and y directions. These types of elements are able to predict plastic deformation, cracking, and crushing. The geometry and node locations for this element type are shown in Figure 4.6.

In 3D models, an eight node linear brick, reduced integration C3D8R element was used to model the concrete. This model has eight nodes with three degrees of freedom at each node, translation in the x, y and z directions. These types of elements are able to predict plastic deformation, cracking, and crushing. The geometry and node locations for this element type are shown in Figure 4.7.

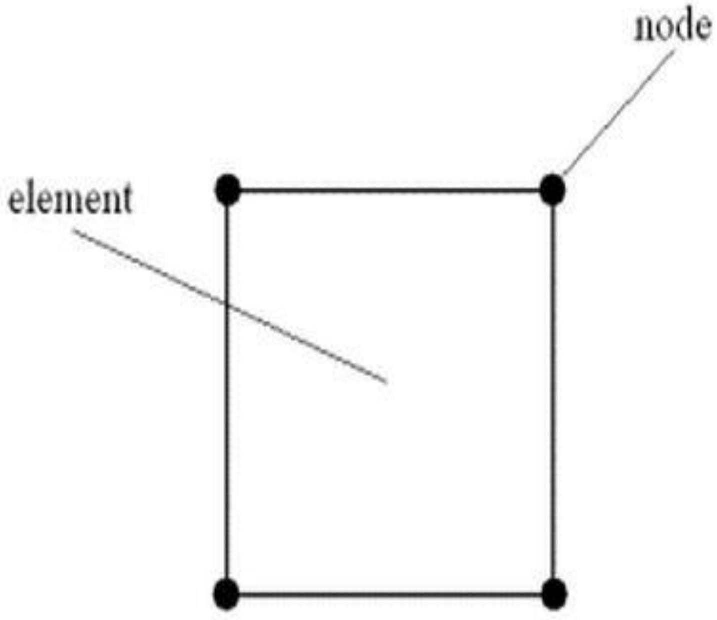

Figure 4.6 Typical Plane Stress Quadrilateral 4 node Element

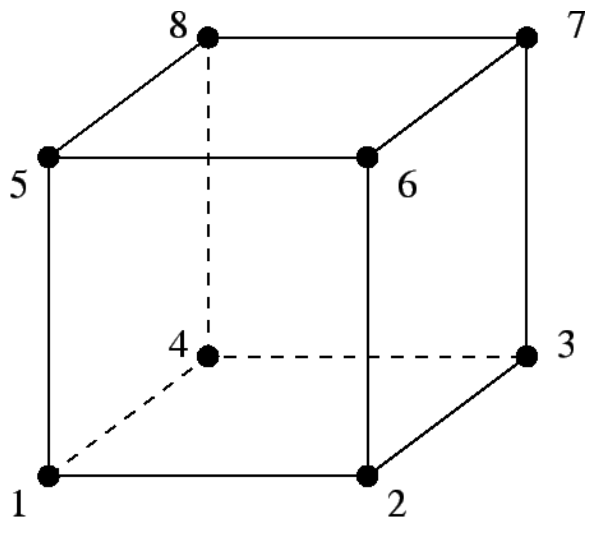

Figure 4.7 Typical 8 nodes Linear Brick Element

4.4.2 Reinforcement

The reinforcement bars were modelled by using both 2D and 3D truss elements. In the 2D model a two node linear T2D2 truss element has been used. In 3D model a two node linear T3D2 truss element has been used. Truss elements are long, slender structural members that can transmit only axial force, see Figure 4.8.

The steel and BFRP reinforcement bars were embedded into the concrete element, hence no interface element was needed and perfect bond between concrete and reinforcement was assumed.

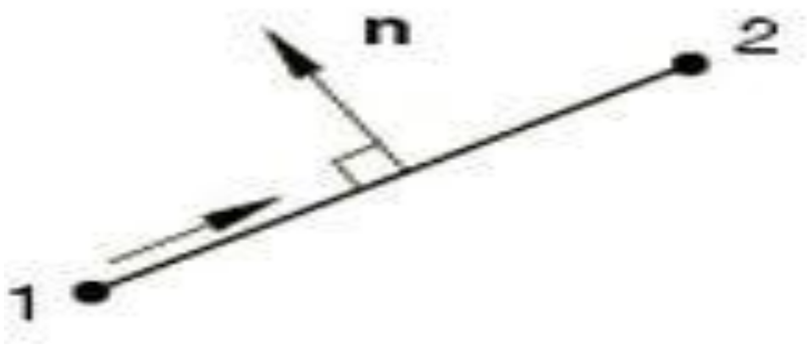

Figure 4.8 Typical 2 Nodes Truss Element

4.5 Material Properties

Any number of materials can be defined in an analysis. Each material definition can contain any number of material behaviours, as required, to specify the complete material behaviour. For example, in a linear static stress analysis only elastic material behaviour may be needed, while in a more complicated analysis several other material behaviours may be required.

4.5.1 Concrete

Concrete is a quasi-brittle material and it behaves differently in tension and compression. Therefore the development of a model to study the behaviour of concrete is a challenging task. Figure below shows a typical stress strain curve for normal weight concrete [57].

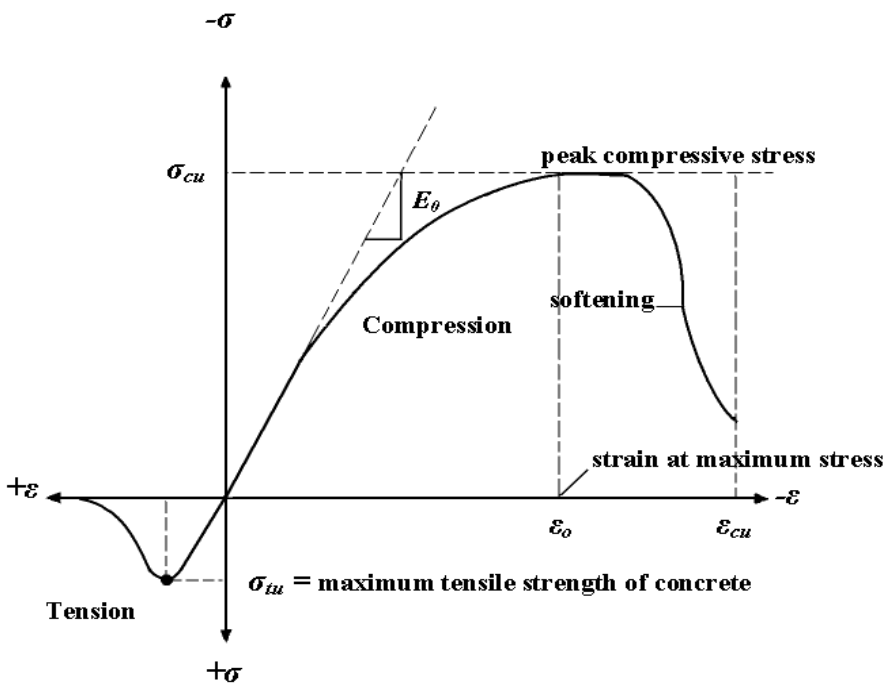

Figure 4.9 Typical Uniaxial Compressive and Tensile Stress Strain Curve for Concrete [57]

In compression, the stress-strain curve for concrete is linearly elastic up to about 30% of the maximum compressive strength. Above this point, the stress increases gradually up to the maximum compressive strength. After it reaches the maximum compressive strength, the curve descends into a softening region, and eventually crushing failure occurs at an ultimate strain.

In tension, the stress-strain curve for concrete is approximately linearly elastic up to the maximum tensile strength. After this point, the concrete cracks and the strength decreases rapidly to zero.

In this study, concrete was modelled using the concrete damage plasticity approach provided in Abaqus. The crack band model was employed because previous research indicated that the smeared crack model has a drawback because it leads to the phenomenon called strain localization which leads to zero energy consumption during crack propagation when the element size approaches zero. One of the successful approaches to deal with this drawback is using a localization limiter such as crack band model [58]. By taking the crack opening displacement w as the cracking strain ε_{cr} accumulated over the width h_c of the crack band as shown in equation (25).

$$w = \int_0^{h_c} \varepsilon_{cr} \, dh \qquad (25)$$

Where: w is crack opening displacement, ε_{cr} is cracking strain and h_c is the crack band width. In Abaqus, h_c can be defined as a crack length of an element. In this study a four node solid CPS4R linear quadrilateral element has been used to model the concrete. Therefore the characteristic crack length has taken to be $\sqrt[2]{e}$, where e is the side length of an element. In this study the side length was taken to be 10mm.

In this study the Poisson's ratio of concrete was assumed to be 0.22 and the density (ρ) is 2400 kg/m^3.

In modelling with concrete damage plasticity there are mainly four sets of parameters that have to be defined. These parameters are concrete compression hardening, concrete tension stiffening, concrete compression damage and concrete tension damage. The concrete compression damage variables were not specified, because it was assumed that there is no stiffness degradation in the compression softening stage.

4.5.1.1 Compression Hardening

The ABAQUS programme requires the uniaxial stress-strain relationship of concrete in tension and compression in order to be able to model concrete. In this study for concrete under compression a relationship proposed by Saenz [59] was adopted as shown in equation (26). See Figure 4.10 and Figure 4.11 for compression hardening relationship for BFRP RC1 and BFRO RC2.

$$\delta = \frac{\alpha\varepsilon}{1+[(\alpha\varepsilon_p/\delta_p)-2](\varepsilon/\varepsilon_p)+(\varepsilon/\varepsilon_p)^2} \qquad (26)$$

In which δ and ε are the compressive stress and strain respectively, δ_p and ε_p are respectively the experimentally determined maximum compressive stress and the corresponding strain, and α is an experimentally determined coefficient representing the initial tangent modulus. In this study, α was set to be equal to the elastic modulus of the concrete E_c and its value was estimated from the cube compressive strength based on the ACI 310 equation (27) in MPa [60].

$$E_c = 4730\sqrt{f_c'} \qquad (27)$$

δ_p and ε_p, were set to be equal to the test value of the cylinder compressive strength f_c' and 0.002, respectively.

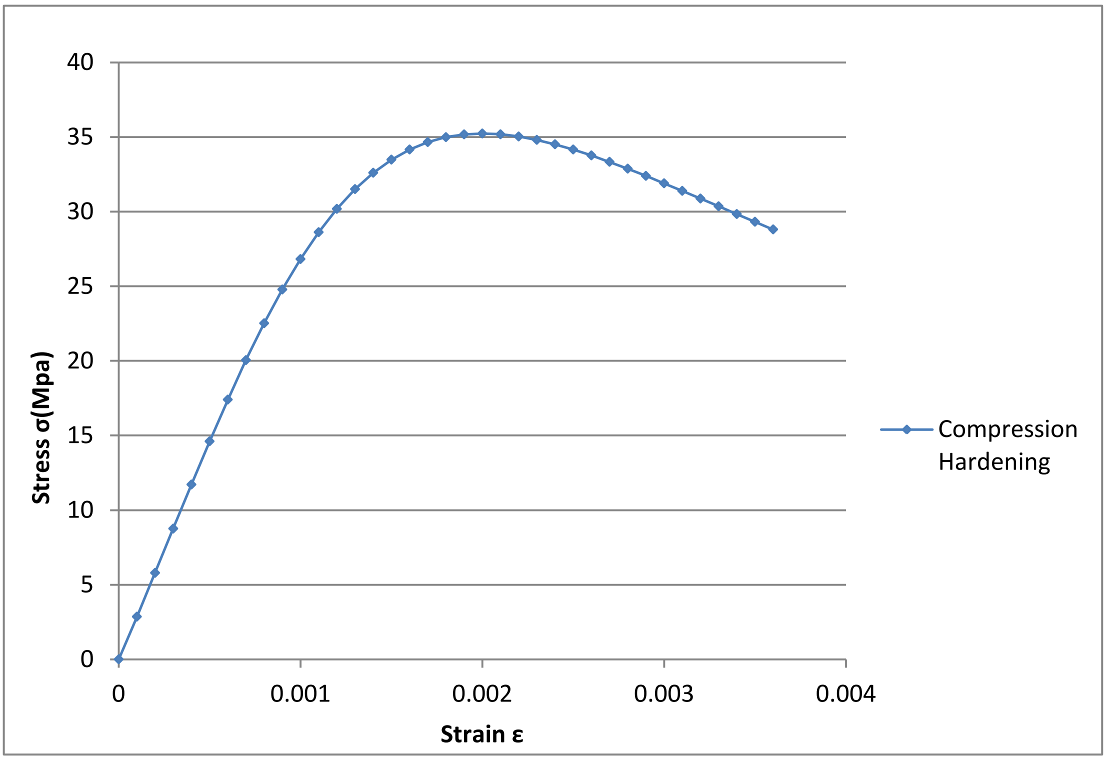

Figure 4.10 Compression Hardening for BFRP RC1

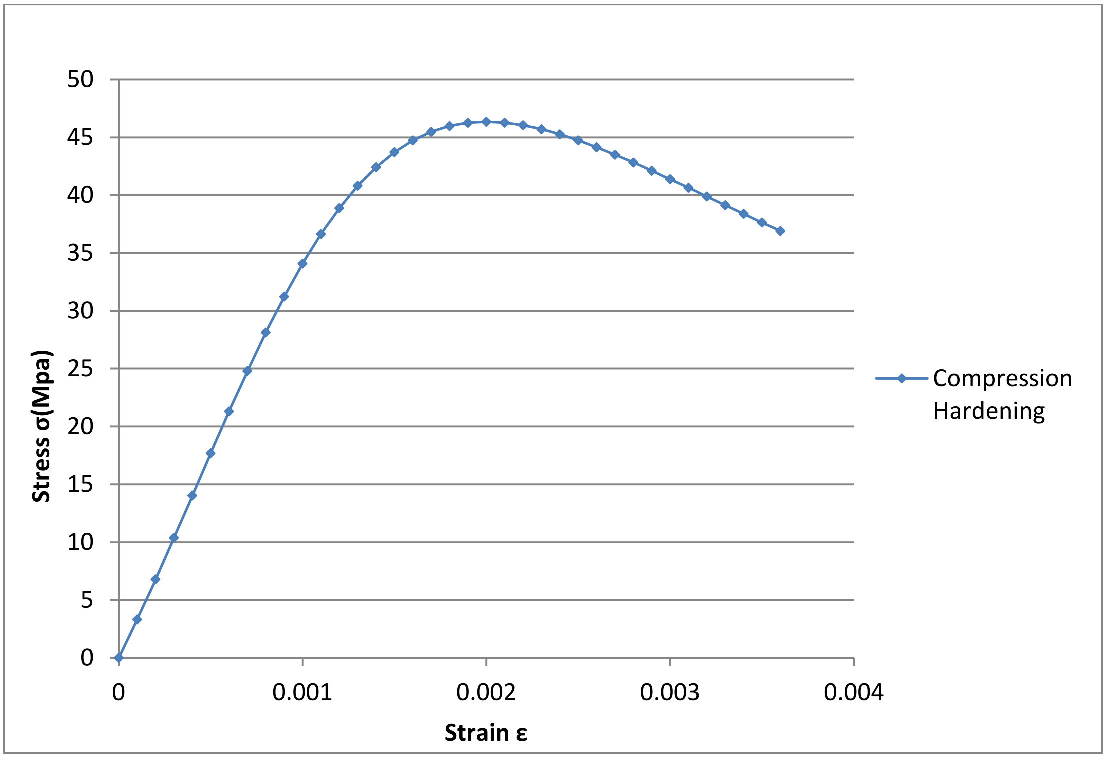

Figure 4.11 Compression Hardening for BFRP RC2

4.5.1.2 Tension Stiffening

The post failure behaviour for direct straining across cracks is modelled within the tension stiffening option, which allows the user to define the strain softening behaviour for cracked concrete. This option also allows for the effect of the reinforcement interaction with concrete to be simulated in a simple manner [61]. See Figure 4.12 and Figure 4.13 for tension stiffening in BFRP RC1 and BFRP RC2.

For concrete under uniaxial tension the tension softening curve of Hordijk [62] which was derived from an extensive series of tensile tests of concrete was employed as follows (28):

$$\frac{\sigma_t}{f_t} = \left[1 + \left(c_1 \frac{w_t}{w_{cr}}\right)^3\right] e^{\left(-c_2 \frac{w_t}{w_{cr}}\right)} - \frac{w_t}{w_{cr}}(1 + {c_1}^3)e^{(-c_2)} \qquad (28)$$

$$w_{cr} = 5.14\frac{G_F}{f_t} \qquad (29)$$

Where w_t is the crack opening displacement, w_{cr} is the crack opening displacement at the complete release of stress or fracture energy, σ_t is the tensile stress normal to the crack direction, f_t is the concrete tensile strength under uniaxial tension, G_F is the fracture energy required to create a stress free crack over a unit area, and c_1=3.0 and c_2=6.93 are constants determined from tensile tests of concrete. In this study f_t and G_F are estimated from equations proposed by CEB-FIP [63].

$$f_t = 1.4\left(\frac{f_{c'}-8}{10}\right)^{\frac{2}{3}} \qquad (30)$$

$$G_f = \left(0.0469{d_a}^2 - 0.5d_a + 26\right)\left(\frac{f_{c'}}{10}\right)^{0.7} \qquad (31)$$

Where, d_a is the maximum aggregate size. The maximum aggregate size was assumed to be equal to 20mm.

A stress displacement curve can be generated from equations (28) and (31) and this can be transformed into a stress-strain curve by using the crack band model as shown in equation (26).

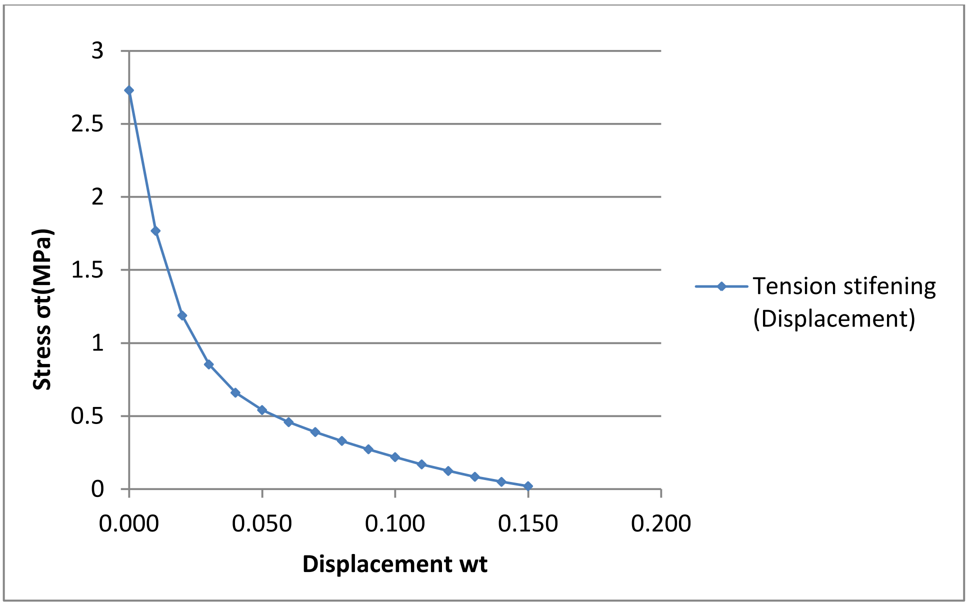

Figure 4.12 Tension Stiffening (Displacement) for BFRP RC1

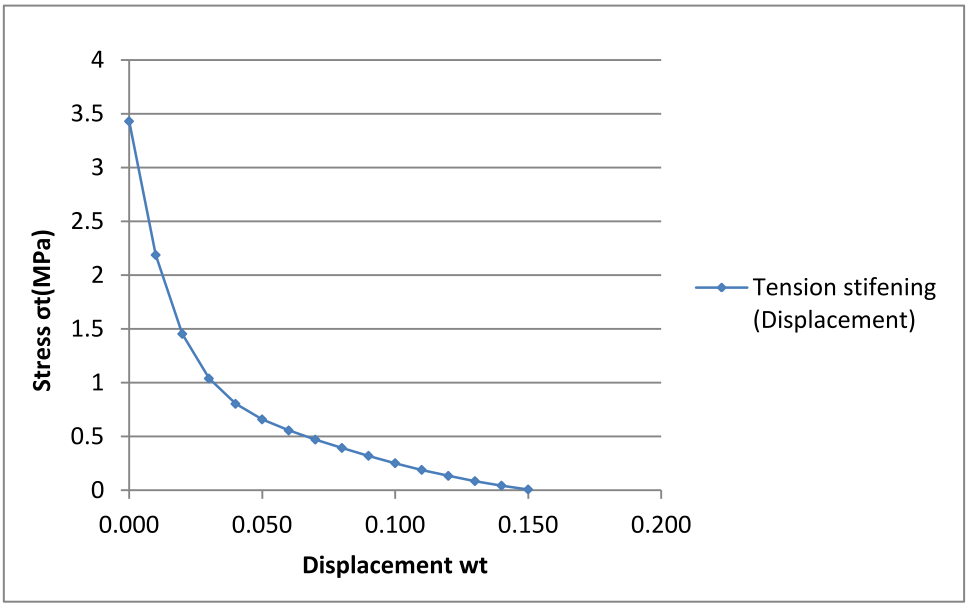

Figure 4.13 Tensions Stiffening for BFRP RC2

4.5.1.3 Concrete Tension Damage

In finding the damage variable, the crack band model was employed to transfer the crack opening displacement w_t into its corresponding crack strain ε_{cr}. Therefore, the relationship of the tensile stress and crack strain was obtained.

In 1988 Rots explained a secant unloading response of concrete in tension which is shown in the above Figure 4.2.a. For secant unloading, the crack normal strain is reversible and upon reaching the origin of the figure the crack truly closes, i.e. ε_{cr} =0, after elastic behaviour is recovered. In this study, the secant unloading response was adopted. The tensile elastic modulus of concrete was assumed to be the same value as the compressive elastic modulus. See Figure 4.14 and Figure 4.15 for concrete tension damage relationship in BFRP RC1 and BFRP RC2.

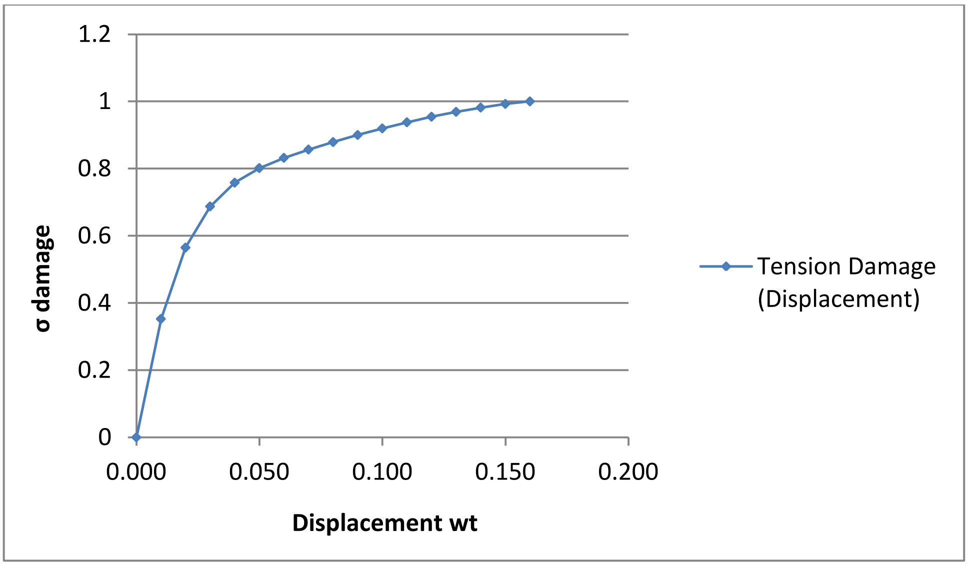

Figure 4.14 Concrete Tension Damage (Displacement) for BFRP RC1

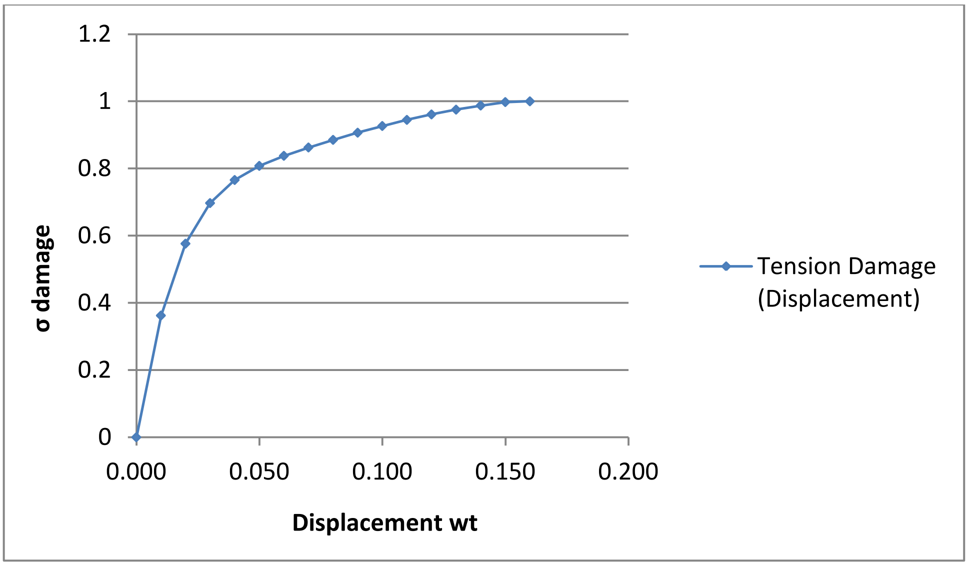

Figure 4.15 Tension Damage (Displacement) for BFRP RC2

4.5.2 Steel Reinforcement rebar

Steel reinforcement in ABACUS modeling assumed to be elastic perfectly plastic material as shown in Figure 4.16. Poisson's ratio was assumed to be 0.3, the elastic modulus was assumed to be 200000 MPa and a yield stress assumed to be 500 MPa.

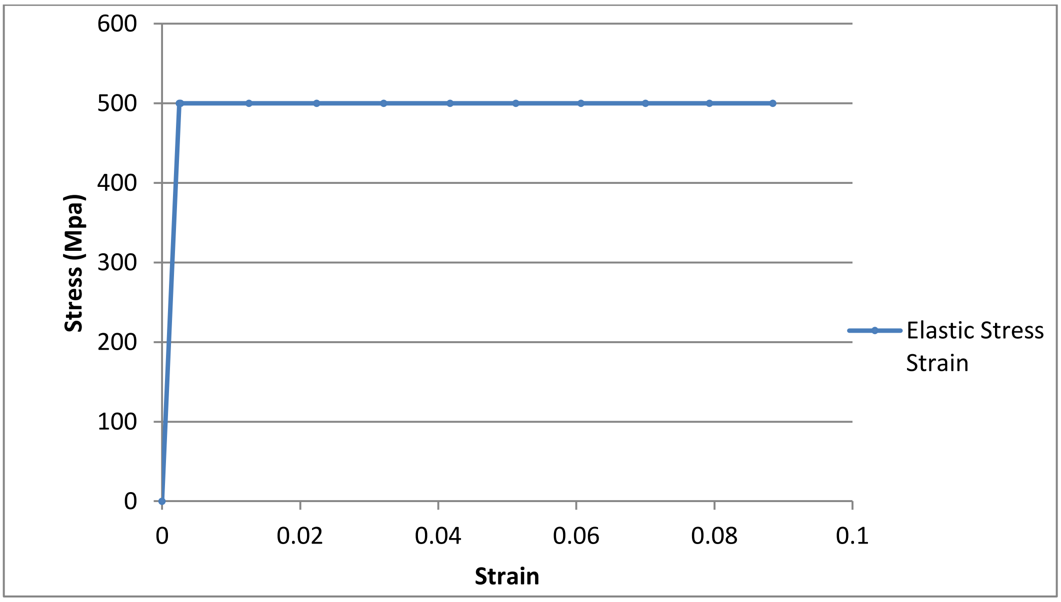

Figure 4.16 Tensile Stress Strain Properties for Steel Reinforcement

4.5.3 Fibre Reinforced polymer (FRP) rebar

BFRP bars are elastic materials up to failure without exhibiting any yield or plastic behaviour. A linear elastic property was used for modelling the BFRP flexural reinforcement. The ultimate stress of BFRP flexural rebar was set to 1350 MPa and the strain to 0.030863 according to tensile tests carried out in the University of Sheffield [49].

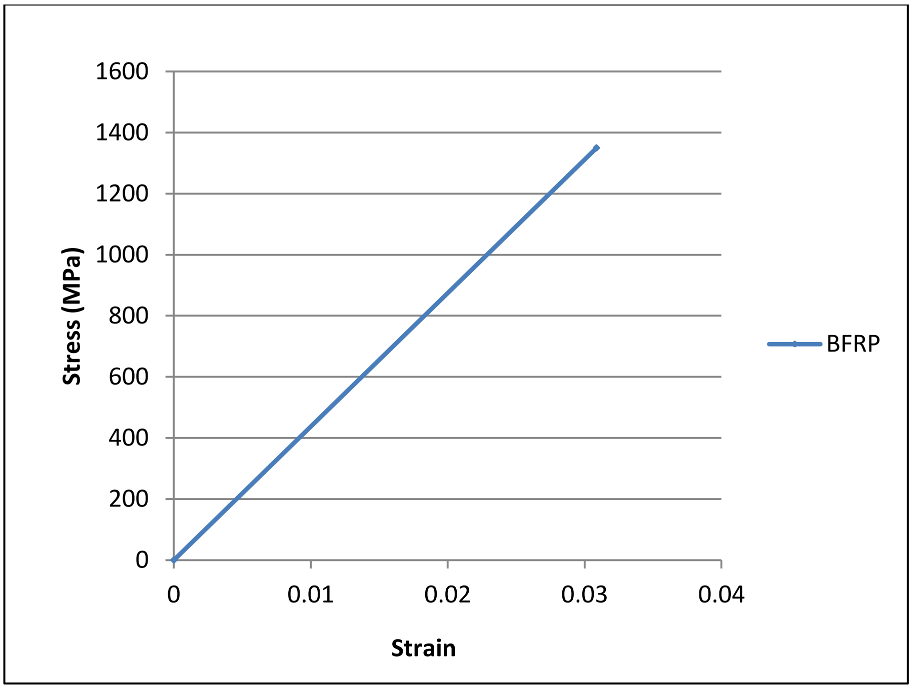

Figure 4.17 Tensile Stress-Strain Property for BFRP Bars

4.6 Geometry

The dimensions of the beams were (150x200x2000) mm. The span between the supports was 1800mm. By taking advantage of symmetry of the beams in the 2D model, half of the full beam was used for modelling but in the 3D model, a quarter of the full beam was used for modelling. This approach reduced computational time and computer disk space requirements significantly. Half of the entire 2D model and a quarter of entire 3D are shown in Figure 4.18.

The bond strength between the BFRP bars and the surrounding concrete was considered as perfect bond. Therefore the embedded option was used in defining the reinforcement inside the host element which was the concrete beam as shown in Figure 4.19.

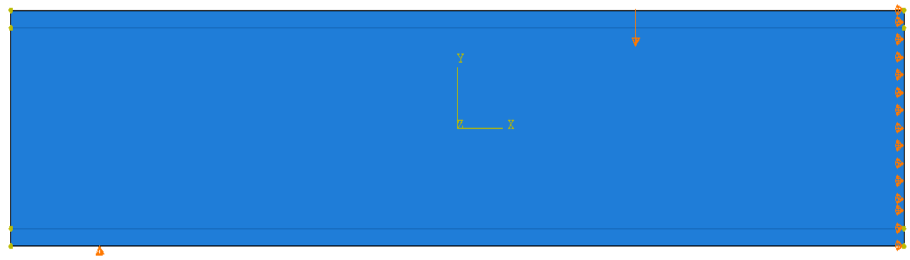

(a)

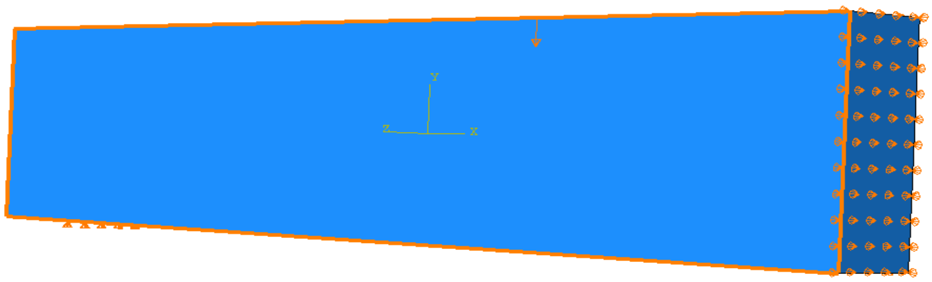

(b)

Figure 4.18 (a) Half of the Beam in 2D Model

(b) Quarter of the Beam in 3D model

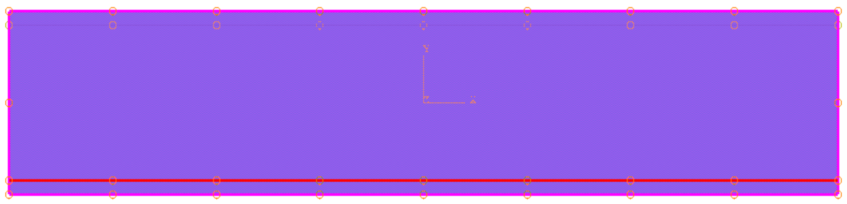

Figure 4.19 Embedding the Reinforcements in the Concrete Element

4.7 Meshing

As an initial step, the finite element analysis requires meshing of the model. Hence, the model is divided into a number of small elements. After the application of the load, the stress and the strain are calculated at integration points of these elements [64]. An important step in finite element modelling is the selection of the mesh density. A convergence of results is obtained when an adequate number of elements are used in a model. This is seen to have been achieved when an increase in the mesh density has a negligible effect on the result. Therefore, it is very important to study the mesh convergence to determine an appropriate mesh density.

Initially, a convergence study was performed using a plain concrete beam in a non-linear analysis. The model worked properly and showed the failure of the beam and an obvious load-deflection curve.

4.8 Loading and Boundary Conditions

The beams were tested under four-point bending. The finite element model was loaded at the same locations as the experimental beam. Because in the two dimensional model half of the entire beam was modelled, and in the three dimensional model a quarter of the entire beam was modelled. Therefore; planes of symmetry were required at the internal faces. At a plane of symmetry, the displacement in the direction perpendicular to the plane was set to zero as shown in below figures.

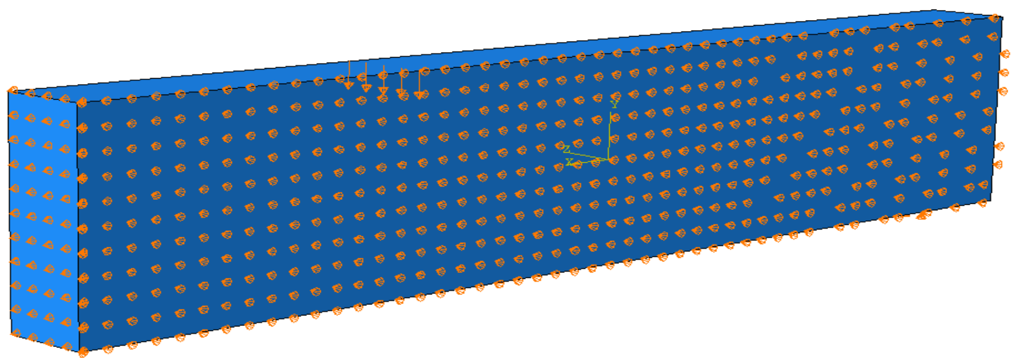

(a)

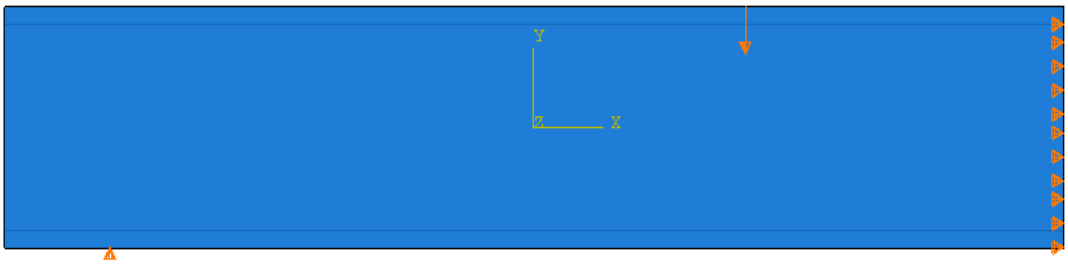

(b)

Figure 4.20 Planes of Symmetry in (a) 3D Model and (b) 2D Model

4.9 Methods for Non-Linear Solution

There are different methods available in Abaqus for finding the solution of non-linear equations such as the linear method, the Newton Raphson method and the modified Newton Raphson method. In this study the modified Newton Raphson method has been used for solving the simultaneous equations and finding incremental equilibrium. This is an iterative process of solving the non-linear equations.

One approach of non-linear solution is to break the load into a series of load increments. The load increments can be applied either over several loads or over several load steps within a load step. At the completion of each incremental solution, the program adjusts the stiffness matrix to reflect the non-linear changes in structural stiffness before proceeding to the next load increment.

The ABAQUS program overcomes this difficulty by using the Full Newton Raphson method, or the modified Newton Raphson method, which drives the solution to equilibrium convergence at the end of each load increment. In the Full Newton Raphson method, it uses the following set of non-linear equations:

$$K(p)\Delta p = q - f(p) \qquad (32)$$

Where q is the vector of total applied joint loads, $f(p)$is the vector of internal joint force, $\Delta p$is the deformation increment due to loading increment, p are the deformations of the structure prior to the load increment and $K(p)$ is the stiffness matrix, relating loading increments to deformation increments.

Figure below illustrates the use of the Newton Raphson equilibrium iterations in non-linear analysis. Before each solution, the Newton Raphson method evaluates the out of balance load vector, which is the difference between restoring forces (the load corresponding to the element stress) and the applied load. The program then performs a linear solution using the out of balance loads and checks for convergence. If convergence criteria are not satisfied the out of balance load vector is re-evaluated and the stiffness matrix is updated then a new solution is obtained. This iterative procedure continues until the problem converges to within defined criteria.

Sometimes the most time consuming part of the Full Newton Raphson method solution is the recalculation of the stiffness matrix $K = (pi - 1)$) at each iteration. In many cases this is not necessary and we can use the matrix $K = (p_0)$from the first iteration of the step. This is the basic idea of the so called Modified Newton Raphson method. It produces very significant time savings. But on the other hand it also exhibits a slower convergence of the solution procedure. The simplification adopted in the Modified Newton Raphson method can be mathematically expressed by:

$K(p_i - 1) = K(p_0)$ (33)

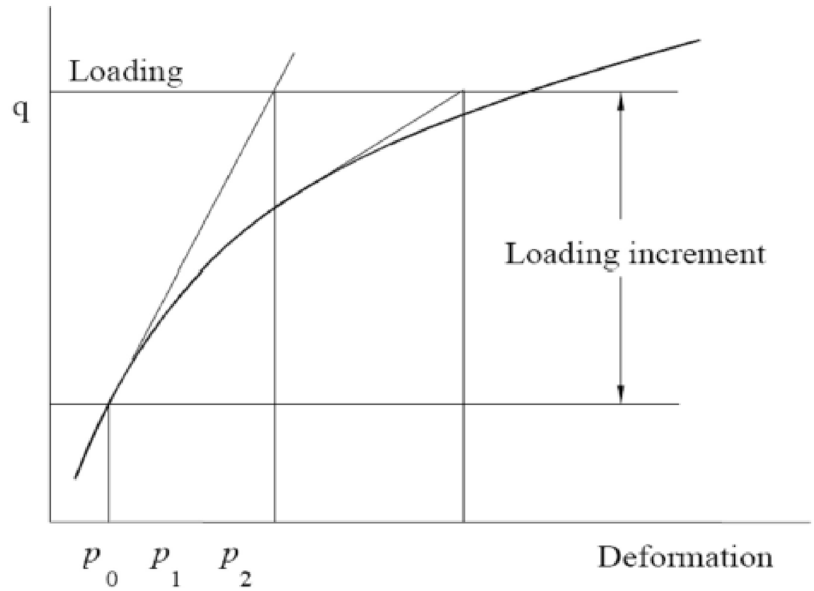

Figure 4.21 Full Newton-Raphson Method

The modified Newton Raphson method which was used in this study is as shown, which when compared to the Full Newton Raphson method it shows that the Modified Newton Raphson method converges more slowly than the original Full Newton Raphson method. On the other hand a single iteration costs less computing time because it is necessary to assemble and invert the stiffness matrix only once. In practice a careful balance of the two methods is usually adopted in order to produce the best performance for any particular case. Usually it is recommended to start a solution with the original Newton Raphson method and later i.e. near extreme points switch to the modified procedure to avoid divergence.

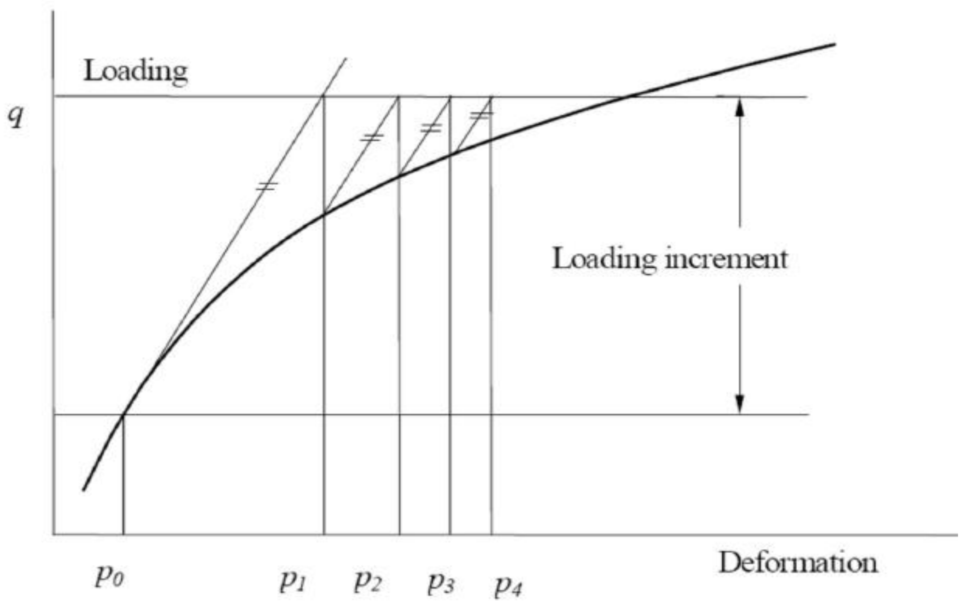

Figure 4.22 Modified Newton-Raphson Method

4.10 Load Stepping and Failure Definition for FE Model

For the nonlinear analysis, automatic time stepping in the Abaqus program predicts and controls load step size. Based on the previous solution history and the physics of the models, if the convergence behaviour is smooth, automatic time stepping will increase the load increment up to a selected maximum load step size. If the convergence behaviour is abrupt, then the automatic time stepping will bisect the load increment until it is equal to a selected minimum load step size. The maximum and the minimum load step sizes are required for the automatic time stepping. In this study when the time period set to 1, the maximum number of increments was 100000, the initial increment size was 0.001, minimum increment size was 1E-015 and the maximum increment size was 0.01.

5 Results and Analysis

5.1 Experimental and Analytical Results

One of the major objectives of this study is the investigation of the flexural behaviour of BFRP RC beams and the applicability of current design guides on the design with BFRP rebar. In this study we compared the capacity and the behaviour of BFRP RC beams to the conventional steel reinforced concrete beams which has the same concrete strength, cross section and reinforcement ratio. Furthermore, a comparison has been carried out of different methods for the determination of ultimate moment capacity and load-deflection relationship of BFRP RC beam.

5.1.1 Moment Strength of the BFRP RC Beam

Based on the test results produced by the University of Sheffield for average and guaranteed properties associated with BFRP RC beam [49], the moment strengths were calculated using both the ACI method and the strain compatibility method.

The compressive strength details for the RC beams and BFRP RC beams are shown in Table 5.1 and the details of properties of steel RC beams and BFRP RC beams are based on average properties of the BFRP bars as presented in Table 5.2.

Table 5.1 Compressive Strength Beams

Beam Designation	m_n (MPa)
S RC1	39.2
S RC2	37.8
BFRP RC1	35.23
BFRP RC2	46.34

Table 5.2 Properties of Beams

Beam	**b** (mm)	**h** (mm)	**d** (mm)	d_c(mm)	**Span** (mm)	**Diameter of Steel Bar** (mm)	**Diameter of BFRP Bar** (mm)	A_{st} (mm^2)	A_{ft} (mm^2)	f_y (MPa)	f_f (MPa)	E_s (MPa)	E_f (MPa)	ε_s	ε_f
S RC1	150	200	174	18	2000	8	8	100.53	93.964	500	1465	200000	47500	0.3	0.030
S RC2	150	200	174	18	2000	8	8	100.53	93.964	500	1465	200000	47500	0.3	0.030
BFRP RC1	150	200	174	18	2000	8	8	100.53	93.964	500	1465	200000	47500	0.3	0.030
BFRP RC2	150	200	174	18	2000	8	8	100.53	93.96	500	1465	200000	47500	0.3	0.030

Table 5.3 presents the experimental moment strength, cracking load, experimental load, experimental deflection and failure mode for basalt reinforced and steel reinforced beams.

Table 5.3 Comparison of steel and BFRP experiments strength

Beam	**Experimental Moment Strength** (kN.m)	**Cracking Load** (kN)	**Experimental Load** (kN)	**Experimental Deflection** (mm)	**Failure Mode**
S RC1	10.2	10.0	34.0	25.6	Tensile Failure
S RC2	10.65	10.5	28.0	25.4	Tensile Failure
BFRP RC1	17.400	11.2	57	73.5	Compression
BFRP RC2	18.3	12.0	61	Gauge Lost	Compression

Table 5.4 presents the moment strengths and cracking loads of basalt beams using different methods.

Table 5. Strength Comparison of BFRP RC Beams Using Different Methods.

Beam	**Moment Strength** (kN.m)			**Cracking Load** (kN)	
	Strain Compatibility	**ACI**	**Experiment**	**ACI**	**Experiment**
BFRP RC1	15.83	16.012	17.400	9.2	11.2
BFRP RC2	18.78	19.031	18.3	11.16	12.0

5.1.2 Load-Deflection Analysis for the BFRP RC Beam

Load-deflection analysis is a very important part for the analysis of reinforced concrete beams especially from the serviceability point of view.

In the literature review chapter it was discussed that FRP materials have a lower modulus of elasticity compared to conventional steel; therefore the deflection limit is a governing parameter in the design of FRP reinforced concrete sections.

A Load-Deflection analysis is the most effective method to predict the moment of inertia of a section after the section has cracked in the tension zone. As soon as the concrete in the tension zone of the concrete beam is cracked this results in the noticeable reduction of the effective moment of inertia which leads to the reduction in stiffness of the section.

Due to the plasticity behaviour of the concrete material and the action of the reinforcement, the concrete beams cannot be analysed using the elastic methods after the concrete is cracked; therefore the prediction of the effective moment of inertia is a very difficult task.

The figure below shows the experimental midspan load-deflection relationship of BFRP RC beams and steel reinforced concrete beams.

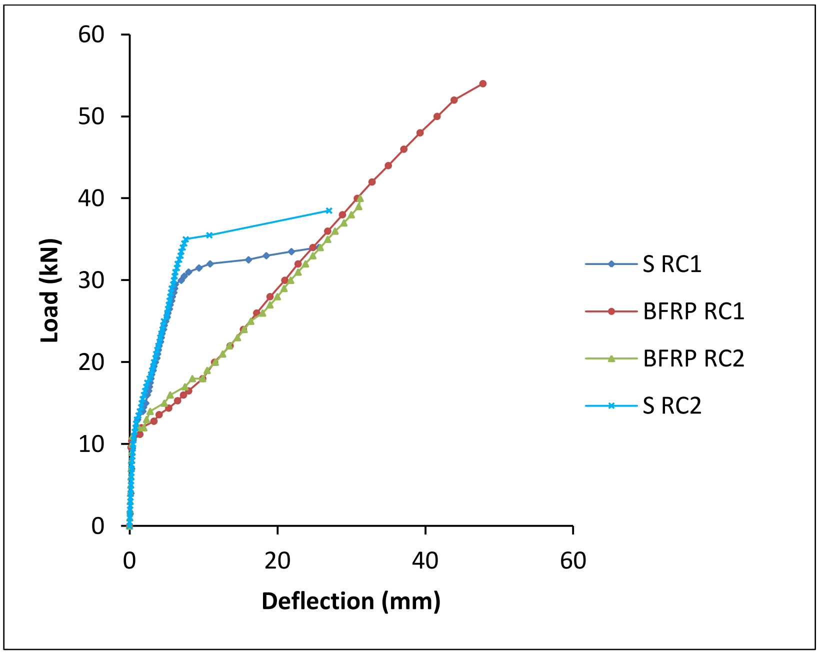

Figure 5.1 Experimental Load – Deflection Curves

In this research a few proposed relationships have been used to compare the prediction of the effective moment of inertia such as original Branson's equation for reinforced concrete beams, the modified Branson's equation and the relationship proposed by Bischoff. These are already discussed in the literature review.

Below figures show the comparison of different proposed theoretical methods for determining the load-deflection relations in BFRP RC beams.

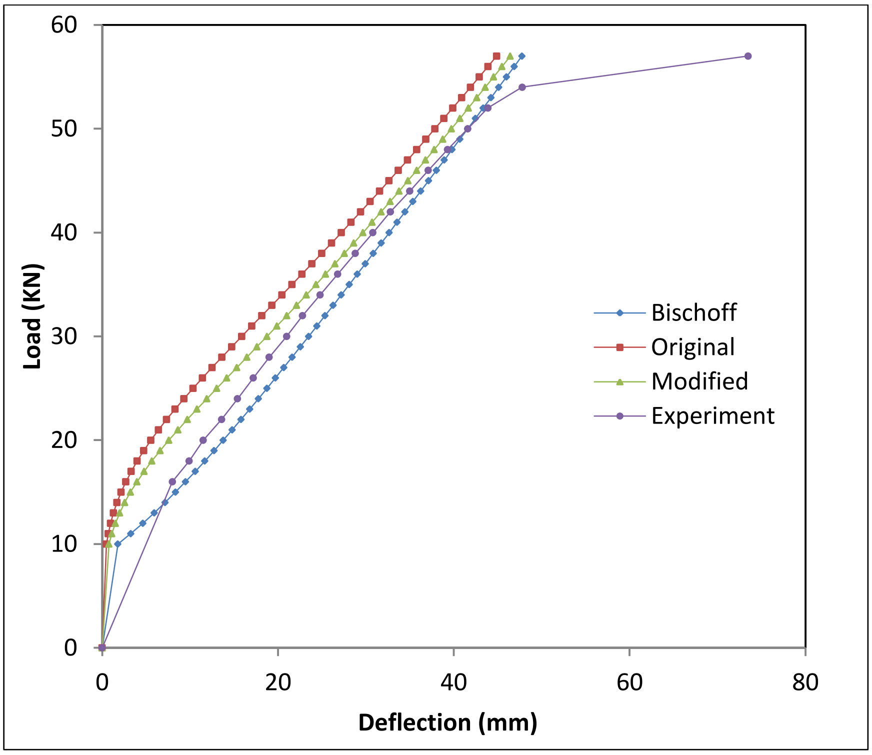

Figure 5.2 Theoretical Load-Deflection Curve for BFRP RC1

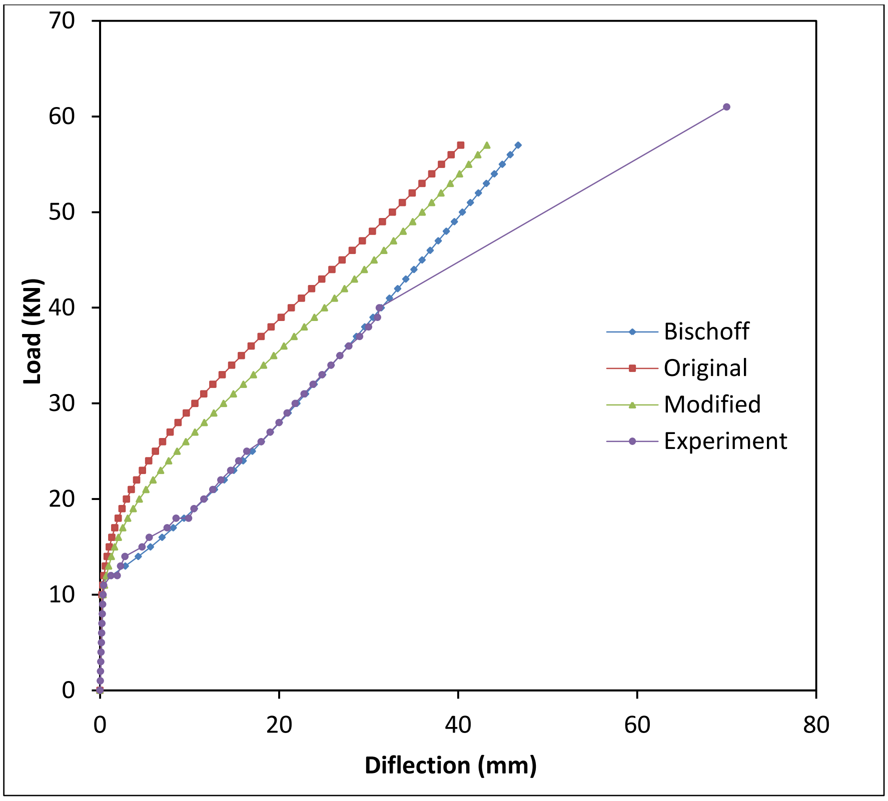

Figure 5.3 Theoretical Load-Deflection Curve for BFRP RC2

5.1.3 Failure Mode

The below figure shows that the failure mode for both BFRP RC beams was in compression of the concrete. When the load applied to the beams in the increment of 0.5kN the deflection was relatively low until the load reached 10kN. Vertical cracks started to develop from the extreme tension fibre zone of the concrete when the load reached 11-12kN. The formation of further vertical cracks also increased and the former cracks propagated and widened as the loading increments went on. When the load reached 15-17kN, the concrete started to fail in tension zone. Beyond that loading, the stiffness of the beam started to decrease. Large deformations started to be observed. Furthermore, diagonal shear cracks developed at each support. When the load reached as high as (45-50) kN in both BFRP RC1 and BFRP RC2 a side way slippage were occurred and continued until the beams failed as shown in Figure 5.4.

Finally both of the BFRP RC1 and BFRP RC2 beams failed in compression at 58kN and 61kN respectively and both beams slipped sideway as shown in Figure 5.5.

Figure 5.4 Failure Mode in BFRP RC beams

Figure 5. Side Way Slipping of the Beams

5.2 FE Results

5.2.1 Load-Deflection Plots

The accuracy of the FE analysis employed in this present study was investigated by modeling a plain concrete beam.

In Abaqus the deflection of the beams was measured in the centre of the bottom face of the beam. The result shows that the model converged successfully and the load-displacement plot is illustrated in Figure 5.6. Furthermore, Figure 5.7 shows failure of the plain concrete beam in tension.

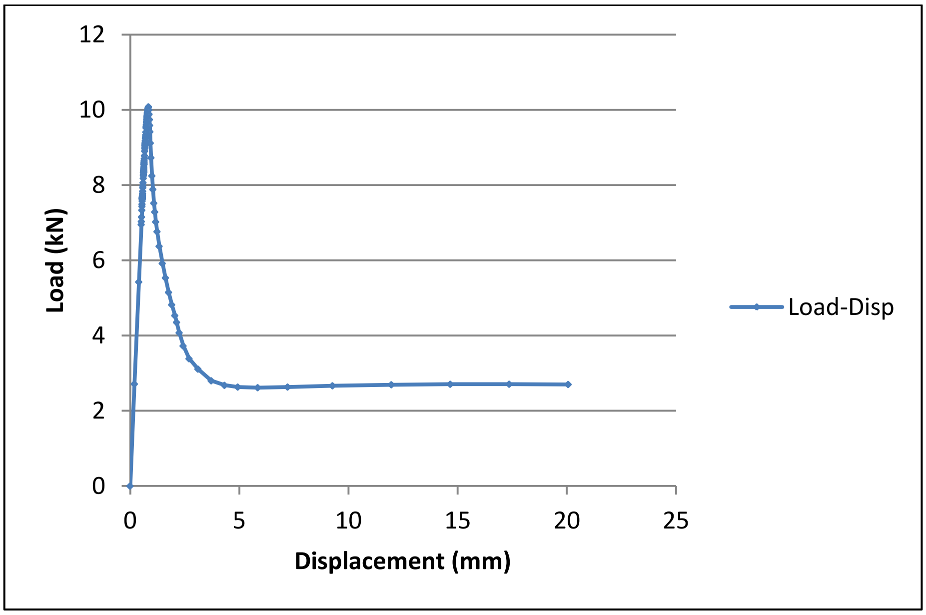

Figure 5.6 Load-Displacement Curve for Plain Concrete Beam

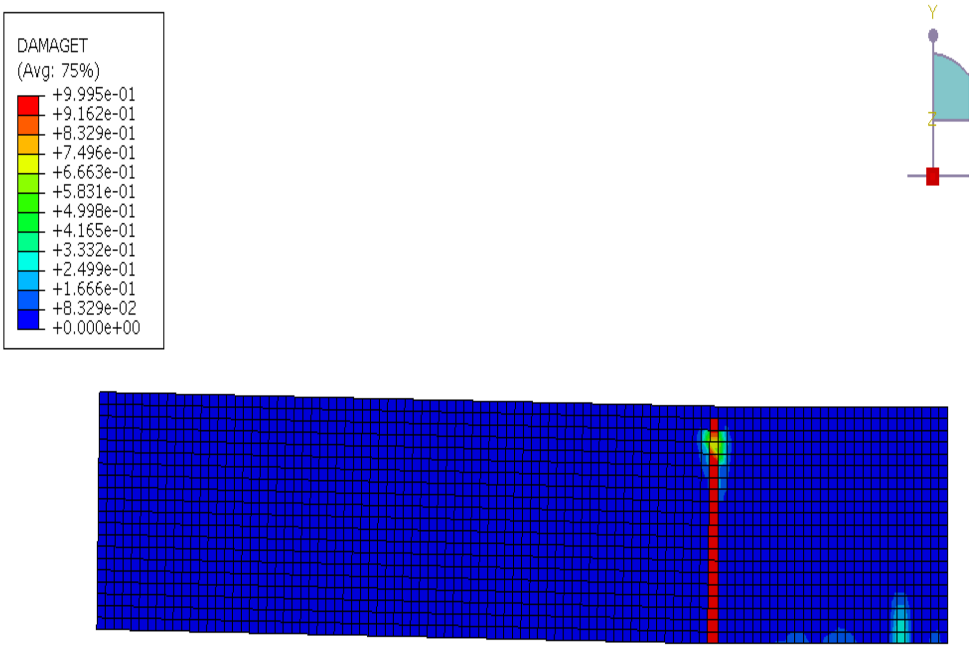

Figure 5.7 Failure of Plane Concrete Beam

The above 2D model for the plain concrete was employed for modelling steel reinforcement beam by introducing steel bar in tension zone and defining the material properties of steel in the Abaqus model. The figure below shows the compression of two dimensional models with the experimental data of steel reinforced beam and the failure of two dimensional steel beams.

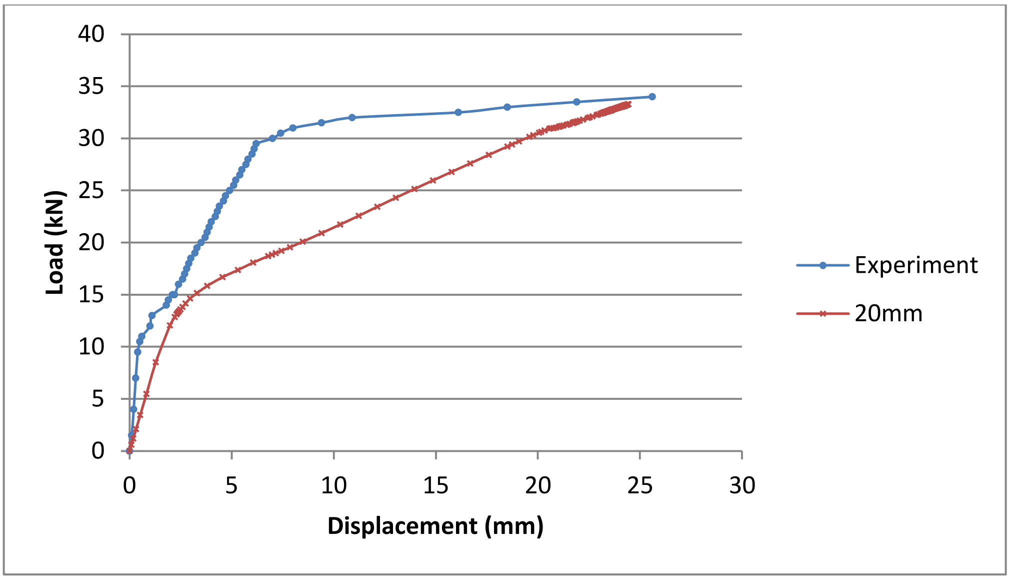

Figure 5.8 2D Modelling of Beam with Steel Reinforcement

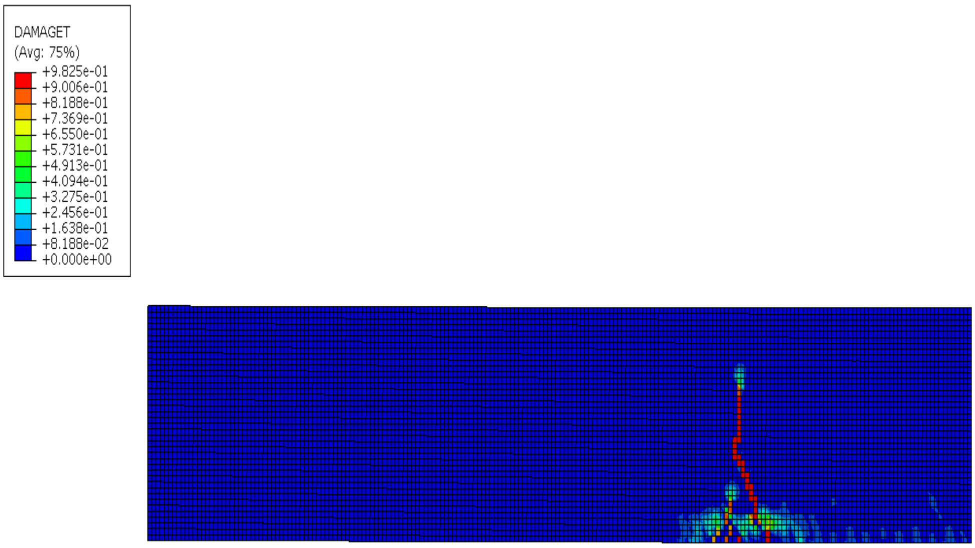

Figure 5.9 Failure of 2D Steel Reinforced Beam

Mesh convergence study with element size 10mm, 20mm and 40mm were carried out for steel reinforced concrete using quarter of the whole beam in the 3D models. The result showed that all the models have had a convergence difficulty as the load goes beyond the maximum as shown in below figure.

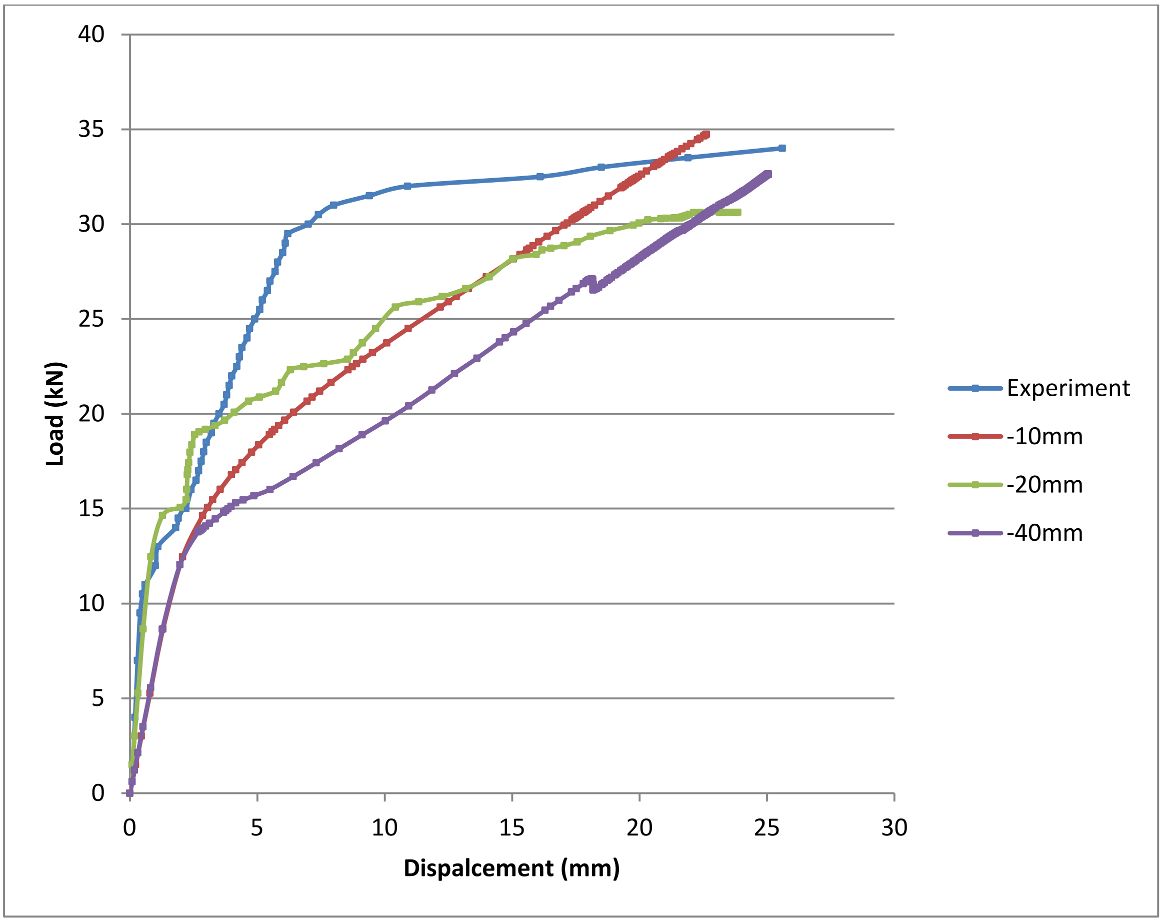

Figure 5.10 3D Modelling of Beam with Steel Reinforcement Using different Mesh Sizes

In the FE modelling of the BFRP reinforced concrete beam using 2D elements, the model presented mesh convergence difficulties when the concrete reaches the plastic stage. Therefore, only the plastic parts model has been generated by Abaqus as shown in the figure.. Also see Figure 5.12 for the elastic deformation of the 2D model.

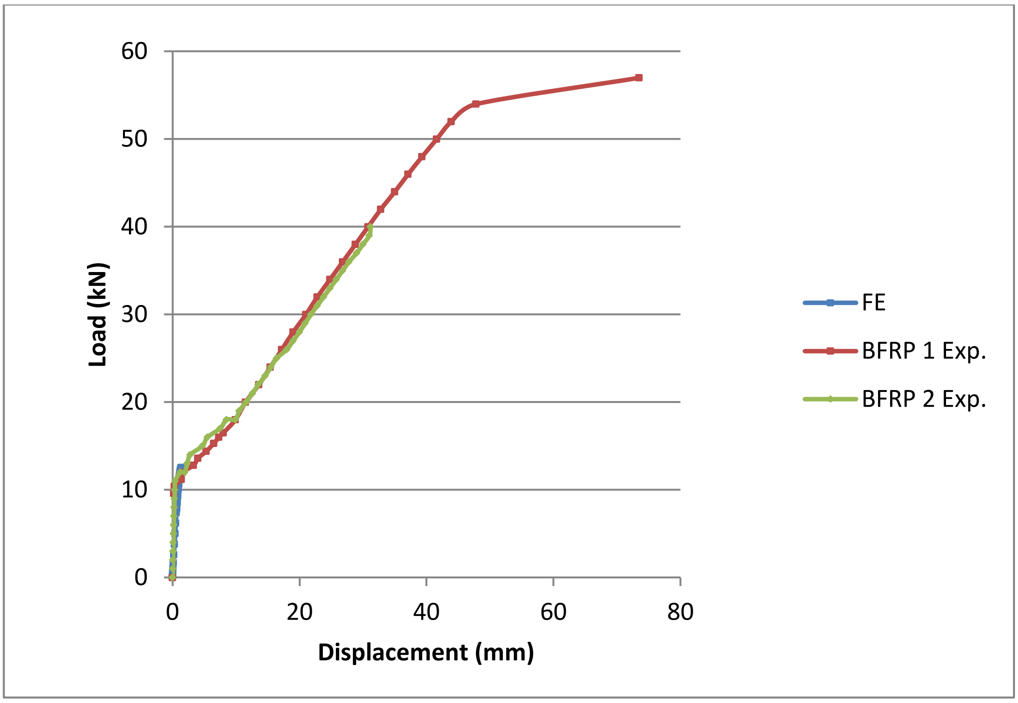

Figure 5.11 2D Modelling of BFRP Beam

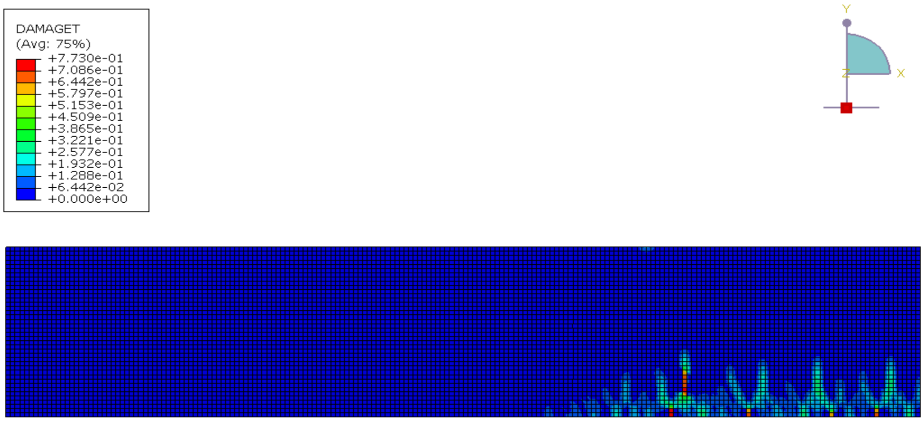

Figure 5.12 Elastic Deformation of 2D BFRP Beam

6. Conclusions and Recommendations

This section presents conclusions that have been determined from studying available alternative materials to replace steel reinforcements in concrete structures. Also includes the conclusion that has been drawn from the four-point bending tests conducted on the BFRP and steel reinforced beams.

The conclusions can be subdivided into the following:

6.1Alternatives to Steel Reinforcement

BFRP bars can be used as an alternative to traditional steel reinforcements in concrete structures, when appropriate strength reduction factor used and the design governed by the serviceability criteria.

Although CFRP has higher elastic modulus and tensile strength compared to BFRP, but the manufacturing of BFRP is more cost effective than CFRP.

GFRP and CFRP approximately have the same mechanical properties. However, BFRP is a better alternative to replace steel reinforcement due to the degradation of GFRP under ultraviolet radiation and moisture absorption.

6.2 Moment Strength of the BFRP Reinforced Beams

From the analysis and tests carried out, it can be concluded that the current design guidelines by ACI committee 440-06 for calculation of moment strength of FRP reinforced concrete beams can predict the moment strength of BFRP reinforced beams. It was also observed that the strain compatibility method can provide a better approximation than the ACI method when concrete strength was slightly higher in BFRP RC2. In both BFRP beams the failure was due to concrete compression and the beams slipped sideways. This probably occurred due to differences in the strengths of the tension bars provided in the tensile zone which made them fail at different times.

6.3 Load-Deflection Analysis of the BFRP Reinforced Beams

From the load-deflection analysis, it was found that the original Branson's equation for determining the effective moment of inertia for the cracked section is under-estimated the deflection of BFRP reinforced beams because it predicted larger section stiffness. It was also observed that the ACI-440 modified equation provided larger section stiffness and under-estimated the deflection of BFRP reinforced beams. Equations proposed by Bischoff [44] provided better approximations for deflections of BFRP beams.

6.4 Finite Element

In the 2D model of half of the steel reinforced beam, the results which are presented in the load-displacement plot show good agreement with predicting the first crack and final load. However, the experimental data indicated greater stiffness for the steel reinforced beam. When the tensile steel bar replaced by BFRP bar the model presented difficulty in mesh convergence. The model could only operate within the elastic range of the BFRP reinforced beam.

The general behaviour of the finite element models for a quarter of the 3D steel reinforced concrete beam, which is represented by the load-displacement plots at the mid-span, did not show good agreement with data provided by the experimental test on the full scale beams. The finite element models showed less stiffness compared to the test data in both the linear and nonlinear ranges. However, the final load and displacement are in a good agreement with the experiments. This is probably due to assumed materials prosperities values instead of measured values from uniaxial tensile and compressive tests. When the steel reinforcement is replaced with BFRP bars in tensile zone, the model showed convergence difficulty at the initial step of analysis.

Further work is required on nonlinear analysis after cracking to model reinforced beams up to failure. The convergence of nonlinear solutions could be improve by using measured materials properties data obtained from uniaxial tension and compression tests.

References

1. Koch, G.H., *Corrosion cost and preventive strategies in the United States*, 2002, Turner-Fairbank Highway Research Center.

2. Balendran, R.V., et al., *Application of FRP bars as reinforcement in civil engineering structures.* Structural Survey, 2002. **20**(2): p. 62-72.

3. R.V. Balendran, T.M.R., T. Maqsood, W.C. Tang, *Application of FRP bars as reinforcement in civil engineering structures.* Structural Survey, 20/11/2002. **20**: p. 62-72.

4. MagmaTech, *RockBar*, *Corrosion resistant basalt fibre reinforcing bars*, 2012, Retrieved 24/5/2012, from http://magmatech.co.uk/downloads/ROCKBAR_4P.pdf: London, United Kingdom.

5. Bank, L.C., *Composites for construction: Structural design with FRP materials*2006: Wiley.

6. Yu.A.Klimon., *A state of the art composite rebar for the reinforcement concrete structures.*, 2010, Kyiv national university of construction and architecture.: Ukraine.

7. Nanni, A., *Composites: coming on strong.* Concrete Construction, 1999. **44**(1): p. 120-124.

8. 440R-96, A.C., *State-of-the-Art report on fibre reinforced plastic (FRP) reinforced for concrete structures*, 2002.

9. Fico, R., *Limit states design of concrete structures reinforced with FRP bars*, 2008, Università degli Studi di Napoli Federico II.

10. Subramanian, D.N., *Sustainability of RRC Structures Using Basalt Composite Rebars.* The Masterbuilder, 9/2010: p. 156-164.

11. Fico, R., *Limit state design of concrete structures reinforced with FRP bars*, in *Material and structures engineering*2010, University of Naples Federico II. p. 167.

12. ACI440.1R-06, *Guide for the Design and Construction of Structural Concrete Reinforced with FRP Bars*, 2006, American Concrete Institute.

13. Karbhari, V.M., et al., *Durability gap analysis for fiber-reinforced polymer composites in civil infrastructure.* Journal of Composites for Construction, 2003. **7**: p. 238.

14. Nanni, A., *Composites: Coming on Strong.* Concrete Construction, 1999. **44**.

15. Bradberry. *Fibre Reinforced Plastic Bar Reinforced Concrete Bridge Decks*. in *Annual Transportation Research Board*. 2001.

16. Rizkalla. *A new Generation of the Third International Symposium on Non-Metallic (FRP) Reinforcement for Concrete Structures (FRPRCS-3)*. 1997.

17. Wu, W.-P., *Thermomechanical Properties of Fibre Reinforced Plastic (FRP) Bars*, 1990, Virginia University, Morgantown, W.Va: Virginia. p. 292.

18. 440.1R, A., *Guide for the Design and Construction of Concrete Reinforced with FRP Bars*, 2003.

19. Bakis, C.E., *Bond of FRP to Concrete for Rods with Axisymmetric Deformations*, in *International Conference on Advanced Composite Materials in Bridges and Structures*1996: Monteral, Canada. p. 853-860.

20. Tighiouart, B., B. Benmokrane, and D. Gao, *Investigation of bond in concrete member with fibre reinforced polymer (FRP) bars.* Construction and Building Materials, 1998. **12**(8): p. 453-462.

21. Schwartz, M.M., *Composite Materials: Properties.* Non-destructive Testing, and Repair, Prentice Hall, NJ, 1997.

22. Bank, L.C., et al., *A model specification for FRP composites for civil engineering structures.* Construction and Building Materials, 2003. **17**(6): p. 405-437.

23. Saafi, M., *Effect of fire on FRP reinforced concrete members.* Composite Structures, 2002. **58**(1): p. 11-20.

24. Hollaway, L.C., *A review of the present and future utilisation of FRP composites in the civil infrastructure with reference to their important in-service properties.* Construction and Building Materials, 2010. **24**(12): p. 2419-2445.

25. Fiber, B., *Composite Materials Technology Development*, Retrieved 24/5/2012, from http://www. basaltfm. com/eng/fiber/info. html.

26. www.withconcrete.com.

27. Clarke, J.L., D.P. O'Regan, and C. Thirugnanendran, *EUROCRETE project: Modification of design rules to incorporate non-ferrous reinforcement.* EUROCRETE Project, 1996.

28. Chris J.Burgoyne, E.B., Maurizio Guadagnini, Gaetano Manfredi, Kyriacos Neocleous, Kypros Pilakoutas, Luc Taerwe , Nicolae Taranu, Ralejs Tepfers, Andre Weber, *Design and use of fibre reinforced polymer reinforcement (FRP) in reinforced concrete structures*, 2007, University of Cambridge.

29. Pilakoutas, K., K. Neocleous, and M. Guadagnini, *Design Philosophy Issues of Fiber Reinforced Polymer Reinforced Concrete Structures.* Journal of Composites for Construction, 2002. **6**: p. 154.

30. Machida, A., et al., *RECOMMENDATION FOR DESIGN AND CONSTRUCTION OF CONCRETE STRUCTURES USING CONTINUOUS FIBER REINFORCING MATERIALS (DESIGN).* Concrete library international, 1997(30): p. 1-64.

31. Bsi, B.S., *8110-1:(1997),".* Structural use of concrete–Part 1: Code of practice for design and construction.

32. Cen, E., *2—Design of concrete structures—Part 1: General rules and rules for buildings*, 1991, ENV 1992-1-1.

33. Canadian Standards, A., *S806-02: Design and Construction of Building Components with Fibre-reinforced Polymers*2004: Canadian Standards Association.

34. Canadian Standards, A., *Design of Concrete Structures: CAN/CSA-A23. 3-04: a National Standard of Canada (approved July 2007),(reaffirmed 2010)*2010: Canadian Standard Association.

35. Association, T.C.S., *Design and construction of building components with fibre reinforced polymers*, 2002, The Canadian Standard Association Ontario. p. 1770.

36. Nanni, A., *Flexural behavior and design of RC members using FRP reinforcement.* Journal of Structural Engineering, 1993. **119**(11): p. 3344-3359.

37. Bakis, C.E., et al., *Fiber-reinforced polymer composites for construction—state-of-the-art review.* Journal of Composites for Construction, 2002. **6**: p. 73.

38. Aiello, M.A. and L. Ombres, *Load-deflection analysis of FRP reinforced concrete flexural members.* Journal of Composites for Construction, 2000. **4**: p. 164.

39. Nanni, A., *Flexural behaviour and design of RC members using FRP reinforcement.* Journal of Structural Engineering, 1993. **119**(11): p. 3344-3359.

40. Branson, D.E. and G.A. Metz, *Instantaneous and time-dependent deflections of simple and continuous reinforced concrete beams*1963: Department of Civil Engineering and Auburn Research Foundation, Auburn University.

41. Nawy, E., *Reinforced concrete: a fundamental approach*2000.

42. Theriault, M., *Effects of FRP reinforcement ratio and concrete strength on flexural behaviour of beams.* Composite for Construction, 1997. **2**.

43. Bischoff, P.H. and R. Paixao, *Tension stiffening and cracking of concrete reinforced with glass fiber reinforced polymer (GFRP) bars.* Canadian Journal of Civil Engineering, 2004. **31**(4): p. 579-588.

44. Bischoff, P.H., *Deflection calculation of FRP reinforced concrete beams based on modifications to the existing Branson equation.* Journal of Composites for Construction, 2007. **11**: p. 4.

45. R.AL-Sunna, R.P., K., Waldron, P. and Al-Hadeed, *Deflection of FRP reinforced concrete beams*, in *4th Middle east symposium on structural composites for infrastructure applications (MESC-4)*2005: Alexandria, Egypt.

46. Rafi, M.M., A. Nadjai, and F. Ali, *Experimental testing of concrete beams reinforced with carbon FRP bars.* Journal of Composite Materials, 2007. **41**(22): p. 2657-2673.

47. Safi, T.a., *Flexural behaviour of concrete beams reinforced with GFRP bars.* ACI Structural Journal, 2000. **97**(5).

48. Adhikari, S., *Mechanical Properties and Flexural Applications of Basalt Fiber Reinforced Polymer (BFRP) Bars.* 2009.

49. Serbescu, A., *Tensile properties of Basalt FRP rebars "Rockbar"*, 2009, Department of Civil and Structural Engineering: The University of Sheffield.

50. 440.3R, A.C., *Finite element analysis of fracture in concrete structures: state of the art*, 1997.

51. Bažant, Z.P. and J. Planas, *Fracture and size effect in concrete and other quasibrittle materials*1998: CRC.

52. Borst, R., et al., *Discrete vs smeared crack models for concrete fracture: bridging the gap.* International Journal for Numerical and Analytical Methods in Geomechanics, 2004. **28**(7-8): p. 583-607.

53. ABAQUS, *ABAQUS/Standard User's Manual*, 2002.

54. Tavárez, F.A., *Simulation of behavior of composite grid reinforced concrete beams using explicit finite element methods*, 2001, UNIVERSITY OF WISCONSIN.

55. Barzegar, *Generating Reinforcement in FE Modeling of Concrete Structures.* Journal of Structural Engineering, 1994: p. 1656-62.

56. Maddipudi, B., *Three-Dimensional Modeling of Concrete Structures* ASCE Journal of Structural Engineering, 1997. **10**(123): p. 1347-1356.

57. Bangash, M.Y.H., *Concrete and concrete structures: numerical modelling and applications*1989.

58. Bazant ZP, P.J., *Crack band theory for fracture of concrete.* Mater Struct, 1983. **16**: p. 155-77.

59. Saenz, L.P., *Discussion of "Equation for the stress-strain curve of concrete," by Desayi and Krishnan.* ACI journal, 1964. **61**(9): p. 1229-1235.

60. Committee, A.C.I., I. American Concrete, and S. International Organization for. *Building code requirements for structural concrete (ACI 318-08) and commentary*. 2008. American Concrete Institute.

61. Hibbitt, K., *Sorensen, Inc. 2002. ABAQUS/standard user's manual, version 6.3. Hibbitt, Karlsson & Sorensen.* Inc., Pawtucket, RI.

62. Hordijk, D.A., *Local approach to fatigue of concrete.* 1991.

63. du Beton, C.E., *CEB-FIP model code 90.* T. Telford, London, 1993.

64. Bathe, K.J., *Finite element procedures*. Vol. 2. 1996: Prentice hall Englewood Cliffs, NJ.